View metadata, citation and similar papers at core.ac.uk

brought to you by CORE

provided by NASA Technical Reports Server

THE UNIVERSITY OF CHICAGO

REMOTE SOUNDING OF STRATOSPHERIC TEMPERATURES USING HIGH RESOLUTION RADIANCE MEASUREMENTS FROM THE IRIS-D

(NASA-CR-141130) REMOTE SOUNDING OF STRATOSPHERIC TEMPERATURES USING HIGH RESOLUTION RADIANCE MEASUREMENTS FROM THE IRIS-D M.S. Thesis (Chicago Univ.) 119 p HC $5.25 CSCL 04A G3/46

N75-13452

Unclas

05017

A DISSERTATION SUBMITTED TO

THE FACULTY OF THE DIVISION OF THE PHYSICAL SCIENCES

IN CANDIDACY FOR THE DEGREE OF

MASTER OF SCIENCE

DEPARTMENT OF THE GEOPHYSICAL SCIENCES

BY

WILLIAM O. GALLERY

CHICAGO, ILLINOIS

DECEMBER, 1974

ACKNOWLEDGMENTS

I would like to thank Dr. Lewis D. Kaplan of The University of Chicago, who originally suggested this project, for his generous assistance and encouragement. I would also like to thank Dr. V. G. Kunde for supplying the transmission data, the IRIS-D radiances, and the *in situ* temperature measurements from the R/NSC. This study was supported by NASA grant NGR 14-001-194.

TABLE OF CONTENTS

LIST OF TABLES

LIST OF ILLUSTRATIONS

LIST OF ILLUSTRATIONS--continued

LIST OF ILLUSTRATIONS--continued

ABSTRACT

Remote sounding of stratospheric temperatures up to 3.2 mb ($\sim$ 40 km) is attempted using high resolution (unapodized) radiance measurements in the 15μ CO_2 band from the Infrared Interferometer Spectrometer on Nimbus 4. Inversions are performed using the Chahine relaxation technique. Radiance data and simultaneous *in situ* temperature profiles are obtained from the Rocket/Nimbus Sounder Comparison. Numerical tests with synthetic radiance data show that the uncertainty in the retrieved temperatures due to random instrument noise is about 1.1 K when averaged over layers about 10 km thick. However, comparison of the measured radiances with the radiances calculated from the *in situ* profiles show the calculated radiances to be systematically higher than the measured radiances. The evidence indicates that systematic errors exist in both the radiance and the *in situ* measurements. These errors are reflected in the temperature profiles, where the discrepancy between the *in situ* and the retrieved temperatures averages 11.5 K at 40 km. Estimates of the possible systematic errors in measured radiances and in the transmission data show that the retrieved profiles may be 6 to 8 K too low at 40 km. This suggests that the *in situ* temperatures may be too high by 4 to 6 K at that height. If the radiance measurements can be corrected for systematic errors, the retrieved profiles may be more accurate than the *in situ* profiles.

INTRODUCTION

Remote temperature sounding from satellites has potentially great value in providing global coverage of the earth's temperature structure. However, up to now most temperature sounding systems have been limited to retrieving temperature no higher than about 20 mb. Extension of this limit to higher in the atmosphere would be of great value to both the forecaster and the basic researcher in stratospheric phenomena.

In this study, I have attempted to obtain remotely retrieved temperatures up to 3.2 mb using high resolution radiance data from the Infrared Interferometer Spectrometer on the Nimbus 4 satellite. Inversion of the radiance data to obtain temperature profiles was done using the Chahine iterative technique. Simultaneous satellite radiance data and *in situ* temperature profiles from the Rocket/Nimbus Sounder Comparison were used, allowing comparison of the inverted profiles with the balloon- and rocketsonde measured profiles. Originally, the program called for obtaining retrieved profiles from the ground up to 3.2 mb. Difficulties encountered in the course of the study, however, limited the retrieved temperatures to the stratosphere only: below the tropopause, *in situ* temperature measurements were used.

The Chahine inversion technique was first evaluated using synthetic radiance data derived from the actual measured profiles. Then real radiance data was inverted and compared to the measured profiles. However, from the comparison of the measured radiances with the radiances calculated

from the *in situ* profiles, it became clear that both the measured radiances and the *in situ* profiles were contaminated with systematic errors. These errors make accurate verification of the retrieved profiles impossible and limit their usefulness.

The principle of obtaining remotely retrieved temperatures up to 3.2 mb from high resolution IRIS data does appear to be valid. If the systematic errors in the radiance data can be reduced sufficiently, then the large amount of data available from this instrument would be available for use in stratospheric research.

THE INVERSION PROBLEM

The outgoing radiation leaving the top of the atmosphere is a complex function of the temperature profile and of the distribution of the absorbing gases present. The inversion problem consists of reconstructing the temperature profile from measurements of the radiance in different spectral intervals, assuming that the distribution of the absorbing gases is known. To understand how this inversion can be accomplished, one must first consider the radiative transfer equation (RTE).

For monochromatic radiation leaving the top of the atmosphere in the vertical (such as is seen by a satellite), the RTE is

$$I(\upsilon) = B(\upsilon,\theta(0))\ T(\upsilon,0) + \int_0^\infty B(\upsilon,\theta(z))\ \frac{dT(\upsilon,z)}{dz}\ dz \qquad (1)$$

where $I(\upsilon)$ is the intensity of radiation emitted at the wavenumber υ, $B(\upsilon,\theta)$ is the blackbody function at the wavenumber υ and temperature θ, $\theta(z)$ is the vertical temperature profile, $z = -\ln(P/P_o)$ is the vertical coordinate, and $T(\upsilon,z')$ is the monochromatic transmission function between the levels $z = z'$ and $z = \infty$. Therefore, $I(\upsilon)$ is a function of the temperature profile $\theta(z)$ and, through the transmission function $T(\upsilon,z)$, of the distribution of the absorbing gases.

If the radiance is measured by an instrument having an instrument function $\phi(\upsilon - \upsilon_i)$ centered on υ_i, the RTE becomes

$$I(\upsilon_i) = \int_0^\infty I(\upsilon)\ \phi(\upsilon - \upsilon_i)\, d\upsilon \qquad (2)$$

If $\phi(\upsilon - \upsilon_i)$ is narrow so that $B(\upsilon,\theta)$ varies little over the width of the instrument function, (2) can be written

$$I(\upsilon_i) = B(\upsilon_i,\theta(0))\ \bar{T}(\upsilon_i,0) + \int_0^\infty B(\upsilon_i,\theta(z))\ \frac{d\bar{T}(\upsilon_i,z)}{dz}\ dz \qquad (3)$$

where the average transmission $\bar{T}$ is

$$\bar{T}(\upsilon_i,z) \equiv \int_0^\infty T(\upsilon,z)\ \phi(\upsilon - \upsilon_i)d\upsilon \qquad (4)$$

Insight into the structure of the RTE can be gained by looking at the form of the function $d\bar{T}/dz$. For an absorbing gas whose mixing ratio is constant with height and whose molecular line intensities depend only weakly on temperature (and, therefore, height), the transmission function is approximated by $\bar{T} = \exp(-cP)$ where c is a constant which depends upon υ_i. Therefore, $d\bar{T}/dz = cP\exp(-cP)$. A typical graph of $d\bar{T}/dz$ vs. z is plotted in Fig. 1. Note that $d\bar{T}/dz$ is strongly peaked around the level marked z_i. Looking at (3), the outgoing radiation can be considered to be (apart from the boundary term) the vertical integral of the blackbody function weighted by $d\bar{T}/dz$. Because of the peaked shape of $d\bar{T}/dz$, the bulk of $I(\upsilon_i)$ comes from the vicinity of the level z_i, with lesser contributions from more distant levels. Thus, as a zero'th order approximation, the temperature $\theta(z_i)$ can be retrieved by calculating the equivalent blackbody temperature of the measured radiance $\tilde{I}(\upsilon_i)$.

However, $d\bar{T}/dz$ is not the best measure of the information carried by $\tilde{I}(\upsilon_i)$. Consider a small increment $\delta\theta(z)$ in the temperature profile $\theta(z)$

and let $\delta\tilde{I}(\tilde{\upsilon}_i)$ be the resulting increase in $I(\tilde{\upsilon})$. It can be shown that when $\bar{T}$ depends only weakly on temperature,

$$\delta I(\tilde{\upsilon}_i) \simeq \int \frac{dB}{d\theta}\frac{d\bar{T}}{dz}\,\delta\theta(z)\,dz \qquad (5)$$

The quantity $\frac{dB}{d\theta}\frac{d\bar{T}}{dz}$ as a function of z represents the sensitivity of $I(\tilde{\upsilon}_i)$ to changes in temperature at the level z. Therefore, the level at which this quantity is a maximum more accurately identifies the level which contributes the maximum information to $I(\tilde{\upsilon}_i)$. The quantity $d\bar{T}/dz$ is called the weighting function, and is the quantity usually presented in remote sounding studies. In this study, $\frac{dB}{d\theta}\frac{d\bar{T}}{dz}$, not $d\bar{T}/dz$, will be called the weighting function for simplicity. Note that the weighting function depends upon the temperature profile. By using a mean or standard atmosphere value for $\theta(z)$, a representative weighting function is obtained.

The temperature inversion problem consists of inferring the vertical temperature profile $\theta(z)$ from a set of measured radiances $\tilde{I}(\tilde{\upsilon}_i)$ at a properly chosen set of wavenumbers $\tilde{\upsilon}_i$. Numerous authors have attempted to solve this problem using a variety of techniques. Westwater and Strand (1972), and Conrath and Reveh (1972) have reviewed the various existing methods. The primary difficulty in the inverse solution of the RTE is that the radiance is a highly nonlinear function of the temperature profile. Attempts to solve the inverse problem by linearization run into the problem that measurement noise renders the solutions physically meaningless. Successful linear methods require the inclusion, either explicitly or implicitly, of *a priori* knowledge of the desired solution.

Chahine (1968, 1970, 1972) however, has developed a very simple nonlinear relaxation technique which he claims requires no *a priori* knowledge of the retrieved solution. The Chahine inversion method starts by assuming an initial guess for $\theta(z)$ and obtaining successively better approximations to the correct profile by relaxation as described below. With n the order of relaxation and $\theta^{(n)}(z)$ the n'th order guess, $\theta^{(n)}(z)$ is used in (3) to calculate $I^{(n)}(\tilde{\upsilon}_i)$. The residuals $R^{(n)}(\tilde{\upsilon}_i)$ are then computed from $I^{(n)}(\tilde{\upsilon}_i)$ and the measured $\tilde{I}(\tilde{\upsilon}_i)$ by

$$R^{(n)}(\tilde{\upsilon}_i) = \left|\tilde{I}(\tilde{\upsilon}_i) - I^{(n)}(\tilde{\upsilon}_i)\right| / \tilde{I}(\tilde{\upsilon}_i) \qquad (6)$$

If the $R^{(n)}(\tilde{\upsilon}_i)$ are of the order of magnitude of the computational and measurement error ε, then $\theta^{(n)}(z)$ is the solution. If the $R^{(n)}(\tilde{\upsilon}_i)$ are greater than ε, then a new guess is generated using the appropriate relaxation equation. The procedure is repeated until the residuals all approach ε or a minimum.

The relaxation equation is derived by considering the equation for $I^{(n)}(\tilde{\upsilon}_i)$, with the boundary term ignored for simplicity:

$$I^{(n)}(\tilde{\upsilon}_i) = \int_0^\infty B(\tilde{\upsilon}_i, \theta^{(n)}(z)) \frac{d\bar{T}(\tilde{\upsilon}_i, z)}{dz} dz \qquad (7)$$

and multiplying it by $\tilde{I}(\tilde{\upsilon}_i)/I^{(n)}(\tilde{\upsilon}_i)$ giving:

$$\tilde{I}(\tilde{\upsilon}_i) = \int_0^\infty \left[B(\tilde{\upsilon}_i, \theta^{(n)}(z_i)) \frac{\tilde{I}(\tilde{\upsilon}_i)}{I^{(n)}(\tilde{\upsilon}_i)}\right] \frac{d\bar{T}(\tilde{\upsilon}_i, z)}{dz} dz \qquad (8)$$

Since $\tilde{I}(\tilde{\upsilon}_i)$ is associated with the temperature at the level z_i of the peak of the i'th weighting function, the new guess for the blackbody function at z_i is given by the expression between the brackets;

$$B(\tilde{\upsilon}_i, \theta^{(n+1)}(z_i)) = B(\tilde{\upsilon}_i, \theta^{(n)}(z_i) \frac{\tilde{I}(\upsilon_i)}{I^{(n)}(\upsilon_i)} \qquad (9)$$

Equation (9) is then solved for $\theta^{(n+1)}(z_i)$ for each υ_i.

The complete relaxation procedure is as follows:

1) Make an initial guess $\theta^{(n)}(z)$, n = 0, which can be almost any function or constant.
2) Calculate $I^{(n)}(\upsilon_i)$ using (7).
3) Calculate $R^{(n)}(\upsilon_i)$ from (6): if all the $R^{(n)}(\upsilon_i) \to \epsilon$, then $\theta^{(n)}(z_i)$ is a solution.
4) If the $R^{(n)}(\upsilon_i)$ are larger than ϵ, generate a new guess $\theta^{(n+1)}(z_i)$ using (9).
5) Using $\theta^{(n+1)}(z_i)$, go back to step 2 and repeat the procedure until all the residuals converge to ϵ.

Note that the convergence of the temperature estimate at one level depends upon the simultaneous convergence of the estimates at all the levels. That is, since $\theta^{(n+1)}(z_i)$ depends upon $I^{(n)}(\upsilon_i)$ which in turn depends upon all the $\theta^n(z_i)$'s, all the $\theta^n(z_i)$'s must converge together, although not necessarily at the same rate. Thus, improvement in the estimate at one level leads to the improvement of the estimates at all levels, but particularly at neighboring levels. This interdependence also implies that

errors, in say one $\tilde{I}(\upsilon_i)$, will affect the retrieved temperatures at not only that particular level, but at neighboring levels also.

As described by Chahine, this procedure is stable against noise in measurements and errors in quadrature. In the presence of random errors in measurement, the solution still converges, and the root mean square residuals R_{rms} converge to an asymtotic value which is of the order of magnitude of the rms errors. Thus, the residuals can distinguish between noise and valid information. In a controlled numerical experiment of inversions done in the 4.3μ region, 2 percent rms random errors in the observed radiances produced an average temperature error of 1 K. Relaxation essentially converges in 10 iterations or less from an isothermal first guess: this number though will depend upon the υ_i's and the number of weighting functions chosen. Also, the final solution does not depend upon the initial guess. Even large errors in the initial guess result in convergence, and all initial guesses converge to essentially the same profile.

However, it should be noted that Chahine's numerical experiments were performed in the 4.3μ region whereas this study uses the 15μ region. The relative variation of the blackbody function with temperature is 3.5 times greater in the 4.3μ region than it is in the 15μ band. This difference between the two bands implies that for the same signal to noise ratio, inversions in the 4.3μ band should give more accurate retrieved solutions than are possible in the 15μ band.

Also, Chahine reports that the iteration should be stopped when the R_{rms} approach a minimum. However, further experience seems to show that

the most accurate solutions are obtained by stopping the iteration at about the point of maximum curvature of the $R_{rms}^{(n)}$ curve (Conrath and Reveh, 1972). This convergence criteria remains somewhat vague, and can best be evaluated by experience.

At this point a note of caution is in order. Chahine's method is based on reducing the residuals, defined by (6), to some small value determined by the measurement and quadrature errors. However, Westwater and Strand (1972) demonstrated that mere smallness of the residuals does not guarantee a solution close to the exact solution. To see this fact, consider the direct problem:

$$I(\upsilon_i) = \int_0^H B(\upsilon_i, \theta(z)) \frac{d\bar{T}(\upsilon_i, z)}{dz} dz, \quad i = 1,2, \ldots M \qquad (10)$$

where $I(\upsilon_i)$ and $\theta(z)$ are exact and H represents the top of the atmosphere. Now consider the integral

$$K(\upsilon_i, N) = \int_0^H [B(\upsilon_i, \theta(z)) + D \sin(\frac{N\pi}{H} z)] \frac{dT}{dz} dz,$$

$$i = 1, \ldots M; \; N = 1,2,3 \qquad (11)$$

where D is an arbitrary constant. By the Rieman-Lebesque lemma (Whittaker and Watson, 1963);

$$K(\upsilon_i, N) \to I(\upsilon_i) \text{ as } N \to \infty, \; i = 1,2, \ldots M \qquad (12)$$

Thus, $K(\tilde{\upsilon}_i,N)$ can approximate $I(\tilde{\upsilon}_i)$ as closely as desired by making N large enough. However, since D is arbitrary, the term in the brackets in (11) can be radically different from $B(\tilde{\upsilon}_i,\theta(z))$. The conclusion to be drawn then, is that the mere convergence of the residuals to some small value does not guarantee that the retrieved profile will be suitably close to the exact profile. Therefore, the use of the smallness of the residuals as a convergence criterion for temperature retrieval is justified only by experiments with real and simulated data.

The particular set of weighting functions is chosen so that the z_i's are evenly distributed throughout the atmosphere. By conservation of information, N radiance measurements can sound no more than N levels in the atmosphere. However, the vertical resolution obtainable is effectively limited by the spread of the weighting functions about the z_i's: if the overlap of two weighting functions is nearly complete, then the information contained in the two radiance measurements at those wavenumbers is largely redundant. Fig. 2 shows one set of seven weighting functions for the 15μ CO_2 band (Conrath, 1972). As shown, there is considerable overlap between weighting functions. Conrath has shown that increasing the number of weighting functions used for inversion from 7 to 16 gains little non-redundant information and consequently only a marginal improvement in the vertical resolution. Furthermore, in the presence of noise in the data, the use of highly redundant weighting functions leads to instabilities in the retrieved profiles. These facts suggest that the largest number of weighting functions that can be usefully employed in temperature inversion in the 15μ CO_2 band is about 10.

THE WEIGHTING FUNCTIONS

The weighting functions selected for use in this study lie in the 15μ CO_2 band. This band is well suited for remote temperature-sounding for several reasons:

1) CO_2 is well mixed in the troposphere and the stratosphere.
2) The band is strongly absorbing, particularly around the Q branches at 667 cm^{-1} and 648 cm^{-1}.
3) Absorption by other gases, such as ozone and water vapor, is small.
4) The temperature dependence of the line intensity, and therefore the absorption is small.

The level at which a particular weighting function peaks is determined by the average absorption within the spectral field-of-view of the spectrometer: the greater the average absorption, the higher the level sounded. In the 15μ CO_2 band, the greatest absorption is due to the lines of the intense Q branch of the υ_2 fundamental vibration-rotation band centered at 667.4 cm^{-1}. These lines are the strongest in the band and are closely spaced. Fig. 3 shows the lines of this Q branch plus a few lines of the P and R branches. The many, much weaker lines from other bands are not shown.

Due to the limited spectral resolution of a conventional satellite spectrometer, its spectral field-of-view must include many lines of varying intensity. The greater the resolution, the more narrowly the instrument

can focus on the strongest lines. By focusing the spectrometer more closely on the strongest part of the Q branch, that is, by using a narrower instrument function, greater average absorption in the spectral field-of-view is obtained. Consequently, the weighting function will peak at a higher level.

Most previous temperature sounding studies have used radiance data from the Satellite Infrared Spectrometers (SIRS-A and B) or the Infrared Interferometer Spectrometers (IRIS-B and D) on the satellites Nimbus 3 and 4. These instruments have a resolution of about 5 cm^{-1} except for the IRIS-D, whose resolution is 2.8 cm^{-1}. As can be seen from Fig. 3, 5 cm^{-1} resolution includes significant regions of low absorption on either side of the Q branch. Fig. 4 gives the weighting functions for the eight channels of the SIRS-A. Note that the weighting function centered at 669 cm^{-1} peaks at about 30 mb. In addition, it is quite broad, making the vertical resolution of the retrieved temperatures in the stratosphere poor. (The IRIS-D weighting functions by Conrath, with 2.8 cm^{-1} resolution, are given in Fig. 2. However, the procedure used to calculate the transmission functions was inaccurate for those weighting functions centered around the Q branch.) In order to get a weighting function which peaks at a higher level, one must go to an instrument with a higher resolving power.

The data from the IRIS can be processed in two ways corresponding to two values of spectral resolution. The IRIS produces raw data in the form of an interferogram which is then Fourier transformed into the radiance spectra. An apodization function may be applied to the interferogram before the Fourier transform is performed. The apodization function has the effect

of reducing the side lobes of the instrument function while at the same time increasing the width of the central maximum. Fig. 5 compares the instrument function with and without apodization. Note that the width of the central maximum of the apodized instrument function is almost twice as large as that of the unapodized one. Thus, the difference between the unapodized and the apodized spectra is that the unapodized radiance $\tilde{I}(\upsilon_i)$ comes from a narrower spectral region around υ_i, but also has more significant contributions from distant regions. The unapodized instrument function also has large negative contributions, whose effect on the weighting functions will be seen later. The resolution of the IRIS-D is nominally 1.4 cm^{-1} in the unapodized mode and 2.8 cm^{-1} in the apodized mode.

Fig. 6 shows the weighting functions at 668.2 cm^{-1} corresponding to both the apodized and the unapodized IRIS-D spectra. Note that the apodized weighting function is sharper and peaks higher than the corresponding SIRS-A weighting function shown in Fig. 4, due to the higher resolution of the IRIS-D. Going from the apodized to the unapodized mode increases this effect further: thus, the hump in the apodized weighting function at around 10 mb disappears. Note also that the weighting function takes on negative values: this effect results from the fact that the unapodized instrument function is significantly negative over certain regions. Using the unapodized IRIS-D spectra, the peak of the highest weighting function is raised to 3.2 mb ($\sim$40 km), up from about 20 mb ($\sim$27 km) for the SIRS-A.

Fig. 7 shows the complete set of weighting functions initially chosen for this study. The transmission data for these weighting functions was supplied by V. Kunde of Goddard Space Flight Center, Greenbelt, Maryland.

He has computed the average transmission due to CO_2 over 0.1 cm^{-1} intervals from 500 cm^{-1} to 800 cm^{-1}, using a detailed line-by-line calculation. The temperature profile shown in Fig. 8 was assumed. The effects of other absorbing gases, such as water vapor, ozone, and nitrous oxide, was not included. The transmissions were computed at 31 pressure levels from 0 to 60 km in steps of about 2 km.

The highest weighting function shown in Fig. 7, using unapodized spectra at 668.2 cm^{-1}, peaks at 3.2 mb. The second highest, also unapodized, is centered at 648.7 cm^{-1} around the Q branch of the υ_2 fundamental of the isotope $^{13}C^{16}O_2$. All the other weighting functions are based on the apodized spectra.

Weighting functions 2 and 3 are actually each based on the difference between two weighting functions. Fig. 9 shows the weighting functions at 668.2 cm^{-1} (unapodized), at 667.5 cm^{-1} (apodized), and the difference between the two curves. The difference curve is seen to have a shape very similar to that of a weighting function. The difference between the two corresponding radiances can be interpreted as follows:

$$I(\upsilon_a) - I(\upsilon_b) = \int_o^\infty \left[B_a \frac{d\bar{T}_a}{dz} - B_b \frac{d\bar{T}_b}{dz}\right] dz \qquad (13)$$

For υ_a = 668.2 cm^{-1} and υ_b = 667.5 cm^{-1} and for θ between 210 K and 300 K, $B(\upsilon_a,\theta) \simeq B(\upsilon_b,\theta)$ to within 0.2 percent. Therefore;

$$I(\upsilon_a) - I(\upsilon_b) \simeq \int_o^\infty B_a \left[\frac{d\bar{T}_a}{dz} - \frac{d\bar{T}_b}{dz}\right] dz \qquad (14)$$

From the shape of the differenced weighting function, $I(\tilde{\nu}_a) - I(\tilde{\nu}_b)$ can be treated as a single radiance which sounds the level of the peak of the differenced weighting function. As shown in Fig. 7, weighting function 2 is based on the difference between the weighting functions at 648.7 cm^{-1} (unapodized) and 655.0 cm^{-1} (apodized), while weighting function 3 is based on 668.2 cm^{-1} (unapodized) and 667.5 cm^{-1} (apodized).

The transmission functions used to calculate the weighting functions do not include the absorption due to either ozone or water vapor. Ozone, which has a maximum concentration at around 20 km, has an absorption band centered at 701 cm^{-1}. By choosing weighting functions on the low wavenumber side of 667 cm^{-1}, instead of the high wavenumber side as in other studies, problems due to the absorption of ozone are avoided.

However, on the low wavenumber side of 667 cm^{-1}, absorption due to water vapor is significant in the lower layers of the atmosphere. Because of the rapid decrease of water vapor amount with height, water vapor absorption at the wavenumber under consideration is negligible above about 400 mb, for standard midlatitude conditions. Below this level, water vapor absorption becomes significant and its effect is to decrease the transmission at any level, compared to the transmission due to CO_2 alone.

Neglecting the absorption due to water vapor in the transmission function leads to errors in the weighting functions and in the calculated outgoing radiance. The level of the peak of weighting functions below 400 mb is underestimated. Since the temperature below 400 mb is in general decreasing with height, the calculated outgoing radiance would be too large.

For these reasons, neglecting water vapor absorption would certainly

lead to errors in the retrieved temperatures in the lower layers of the atmosphere. On the other hand, I hoped that these errors would not be too large and would be confined to the lower layers, with little effect on the retrieved temperatures in the upper layers. However, when inversions were performed using the full set of weighting functions shown in Fig. 7, gross instabilities in the retrieved temperatures in the lower levels appeared which propagated to the highest levels and rendered the retrieved profiles meaningless.

To correct this problem by including water vapor absorption in the transmission function would be beyond the scope of this study. So to overcome this difficulty, I decided to include only those weighting functions peaking above the tropopause in the relaxation procedure. Below the tropopause, the retrieved profile is merged into the *in situ* profile in order to calculate the outgoing radiance. Since the aim of this study is primarily to retrieve temperatures in the stratosphere, eliminating the retrieval of tropospheric temperatures in not a great loss.

So far, little has been said regarding the accuracy and the vertical resolution of the retrieved profiles. Conrath (1972) has shown that for a given level of noise in the measured radiance, there is a trade-off between accuracy and vertical resolution: increased accuracy can be achieved only at the expense of decreased vertical resolution. In order to investigate this effect, the following calculation was performed: using an assumed temperature profile $\theta_0(z)$, the outgoing radiance $I_0(\upsilon_i)$ was calculated for each υ_i. Then at each of the thirty 2 km thick layers z_j, a 2 K perturbation was added to $\theta_0(z_j)$ and the radiance $I_j(\upsilon_i)$ calculated. The

residuals $R_j(\tilde{\nu}_i) = (I_j(\tilde{\nu}_i) - I_0(\tilde{\nu}_i))/I_0(\tilde{\nu}_i)$ are shown in Table 1.

The maximum residuals are about 0.5 percent for the lower weighting functions, decreasing to about 0.2 percent for the highest. These residuals should be compared to the instrument noise of about 1 percent. Clearly a 2 K error in the retrieved profile in a layer 2 km thick could not be detected to within the measurement error. In order to produce residuals comparable to the instrument noise, the vertical resolution must be degraded to about 4 to 5 km for the lower weighting functions and to as much as 8 km for the highest. Conversely, for a vertical resolution of 2 km, the minimum uncertainty of the retrieved profiles must be increased to about 5 to 10 K. Note that these trade-off figures include contributions only from the measurement error; the inversion routine itself will introduce further uncertainties into the retrieved profiles.

Clearly the spacing between weighting functions 3 and 4 in Fig. 7 ($\sim$2 km) is too small for a reasonable level of accuracy in the retrieved profile. Therefore, I decided to limit the number of weighting functions in the stratosphere to three. Also, the measurement error for a combination weighting function is twice that for a single one, since the error in the individual radiances add. Therefore, I further decided to drop the combination weighting functions and use only the single radiance form.

Fig. 10 shows the final set of weighting functions chosen for this study. An additional one (667.4 cm^{-1}, apodized) is shown which is not used in the relaxation: however, since this channel sounds practically the entire stratosphere, its radiance provides a useful check on the internal consistency of the retrieved profiles.

ROCKET/NIMBUS SOUNDER COMPARISON

The radiance and temperature data used in this study were taken from the Rocket/Nimbus Sounder Comparison (R/NSC)(Rocket/Nimbus Sounder Comparison, 1972). In this experiment, conducted during the summer of 1970 at Wallops Island, Virginia, *in situ* temperature measurements were made coincident with radiance measurements by the IRIS-D and the SIRS-B instruments on the Nimbus 4 satellite passing overhead. The objectives of the study were to compare the compatibility of:

1) radiance data derived from different satellite spectrometers;
2) temperatures measured by balloonsondes and different types of meteorological rockets, and,
3) satellite retrieved profiles and *in situ* measured temperatures.

In designing the experiment, care was taken that the satellite systems and the balloon- and rocketsondes were measuring essentially the same environment. Usually, the satellite did not pass directly overhead of Wallops Island. Therefore, the criterion for making observations was established that the distance between the *in situ* observations and the satellite path be less that ±5° of longitude. A maximum time difference in observations of one hour was set. However, there is a difference in the sampling properties of the two systems: the balloon- and rocketsonde measurements

are local values taken along the trajectory of the vehicle, while the IRIS-D measures the average radiance over a vertical column about 120 km in diameter. The differences in the sampled environment due to horizontal temperature differences were minimized by making the measurements in the summer, when the horizontal temperature gradients in the stratosphere are quite weak (as little as 15 K from equator to pole).

The *in situ* temperature profiles are derived from combined balloon- and rocketsonde measurements. The balloonsonde measurements are used up to about 20 km where they are merged with the rocketsonde profiles, which extend up to about 60 km.

There is considerable uncertainty regarding the accuracy of the *in situ* profiles. The balloonsonde temperatures are considered to be accurate to better than ±1 K up to about 20 km. Analysis of the rocketsonde data is complicated by the fact that three different instrument packages were used and there are systematic differences among their measured temperatures. Further, the measured temperatures must be corrected for various effects, such as radiative heating and conductive heat transfer. As many as 40 parameters are involved in the temperature correction, and because the values of many of these parameters are poorly known, the accuracy of the measured temperatures is uncertain. Estimates of the uncertainty in one instrument are: 1 K from 25 to 40 km, about 3 K at 50 km, and about 8 K at 60 km.

Comparison of rocketsonde and satellite measurements indicate systematic differences between the two, with the rocketsonde values being higher. This point will be discussed in much greater detail later.

Simultaneous *in situ* temperature profiles and IRIS-D radiance data for nine days in June and July of 1970, were provided by V. Kunde. The temperature data were smoothed and interpolated to give the mean temperature in each 2 km thick layer from the ground to 60 km. The radiance data are given at discrete wavenumber intervals. Due to the effects of off-axis rays in the interferometer, a wavenumber correction, amounting to 0.3 cm^{-1}, must be added to the tabulated wavenumbers to obtain the true values. The weighting function center wavenumbers υ_i were adjusted slightly to coincide with the corrected tabulated values and new weighting functions were calculated. The new weighting functions were negligibly different from the old. The noise equivalent radiance of the IRIS-D is estimated to be about 0.5 erg $sec^{-1}cm^{-2}str^{-1}/cm^{-1}$ (hereafter called simply ergs) in the apodized mode, and somewhat more in the unapodized mode (Hanel *et al.*, 1972). Typical measured radiances are about 50 to 70 ergs, so that the noise is about 1 percent.

The precision of the radiance measurements vs. the *in situ* temperature measurements has been compared by Kunde *et al.* (1974). The standard deviation of the brightness temperature in the region 600-750 cm^{-1} for eight Wallops Island cases was about 1 K. The standard deviation of the corresponding *in situ* temperature measurements averaged over the 0-50 km range was about 3 K, indicating a lower precision in the *in situ* measurements compared to the satellite measurements.

THE DIRECT PROBLEM

Each iteration of the relaxation procedure requires the solution of the direct problem; that is, the calculation of the outgoing radiance from a given temperature profile using (3). Since the calculation must be repeated many times, a rapid but accurate algorithm must be found. The transmission data $\bar{T}(\upsilon,z)$ is given at 0.1 cm^{-1} intervals in υ, and at 31 pressure levels in steps of about 2 km, from the ground to 60 km. Replacing (3) with a simple numerical quadrature, and ignoring the boundary term for now, the direct problem becomes

$$I(\upsilon_i) = \sum_j \sum_\ell B(\upsilon_\ell, \theta(z_j))\ \Delta\bar{T}\ (\upsilon_\ell, z_j)\ \phi\ (\upsilon_\ell - \upsilon_i) \qquad (15)$$

Now the unapodized instrument function dies out slowly; its envelope does not become less than one percent of its maximum value until about 40 cm^{-1} away from the center. Letting the limits of the integration in υ be $\upsilon_i \pm 40$ cm^{-1}, there are 800 quadrature points in υ. The integration with respect to z involves 30 quadrature points. Performing the double summation indicated in (15) for each iteration of the relaxation scheme and for each υ_i would require large amounts of computing time and storage.

Appendix A gives an efficient algorithm for evaluating (15) which uses an approximate factoring of the blackbody function. Factoring the blackbody function into terms containing υ and θ alone allows the integration with respect to υ in (15) to be done once and for all. The calculation of

$I(\sigma_i)$ requires only the integration with respect to z, reducing the computation time required to solve the direct problem by a factor of about 800. For a given profile $\theta(z_j)$, j = 1, 30, the quadrature error in the calculated radiance associated with the factored blackbody approximation is less than 0.4 percent.

However, there is a remaining difficulty associated with the emission from the top-most layer of the atmosphere. In the supplied transmission data, the transmission at the 60 km level has been taken to be identically equal to 1. For most spectral intervals, this approximation is quite good since the absorption above 58 km is negligible. However, for the unapodized weighting functions centered at 668.1 cm^{-1} and 648.6 cm^{-1}, the absorption above 58 km is 9 and 1.7 percent respectively. For these two channels, the emission from above 58 km is a significant fraction of the total.

In calculating the outgoing radiance, the contribution from each atmospheric layer is given to a close approximation by multiplying the blackbody function at the average temperature of the layer by the change in transmission in that layer. The average temperature of the layer is taken as the temperature at the center of the layer. With the given transmission data however, the layer above 58 km actually extends up indefinitely, and there is no clear definition of the average temperature of this layer.

It is possible to place limits on the range of possible values for the effective emission temperature of this layer, call it $\theta(z_T)$. Appendix B discusses the problem of determining $\theta(z_T)$ and shows that its range is limited to about 220 ± 20 K. For this study, the value of $\theta(z_T)$ = 220 K was adopted. The corresponding uncertainty in the calculated outgoing

radiance due to the uncertainty in $\theta(z_T)$ is ±2 ergs for the highest weighting function corresponding to $\tilde{\nu}_1$, and much less in the other channels. The effect of this uncertainty will be considered later.

Having established the value of $\theta(z_T)$, the outgoing radiance can be calculated from the *in situ* temperature profile and the results compared to the measured radiances. The measured and calculated radiances should agree to within experimental and computation error. Table 2 compares the measured and calculated radiances for the nine days of data. The calculated radiances are systematically higher than the measured radiances by from 5 to 20 percent. The most significant discrepancy is in $I(\tilde{\nu}_i)$, where the average difference is 11.9 ergs.

The same difficulty was noted by Kunde *et al.* (1974), in their comparison of the calculated and the measured radiances using the apodized IRIS spectra. The authors noted three possible sources for this discrepancy: 1) theoretical transmittances; 2) absolute instrument calibration, and, 3) *in situ* temperature measurements. These and other possible sources of error will now be examined to see if the difference between the calculated and the measured radiances can be accounted for. First, errors in the calculated radiance will be considered.

The uncertainty in the CO_2 transmission functions has been estimated to be 5-10 percent (Kunde and Maguire, 1974). A 10 percent uncertainty in the transmission implies about a 10 percent uncertainty in the level P′ of the peak of the corresponding weighting function. For weighting function 1, peaking at 3.2 mb, a 10 percent uncertainty in P′ corresponds to an uncertainty in the temperature at P′ of about ±1.5K. Translating this uncertainty in $\theta(P')$ roughly into the uncertainty in the radiance for that

weighting function gives a possible error in $\tilde{I}(\tilde{\nu}_1)$ due to transmission errors of at most ±2 ergs. A more likely error would be ±1 erg.

The uncertainty in $\theta(z_T)$ contributes at most another 2 ergs to the uncertainty of the calculated radiance. But this again is a maximum estimate and would require a value for $\theta(z_T)$ of 200 K. Again, a more likely uncertainty in the calculated radiance due to $\theta(z_T)$ is ±1 erg.

Finally, Hanel *et al.* (1971) states that, instead of the nominal resolution of the IRIS-D spectra of 1.4 cm^{-1}, the actual resolution is 1.8 cm^{-1} due to the natural apodizing effect of the off-axis rays in the interferometer. In calculating the radiance, however, the unapodized instrument function of resolution 1.4 cm^{-1} was assumed. It is estimated that using this instrument function could lead to calculated radiances systematically too high by 2 ergs, at 668.1 cm^{-1}.

Now consider possible systematic errors in the radiance measurements. The absolute calibration of the IRIS-D has been estimated by comparing simultaneous IRIS-D and SIRS-B measurements during the R/NSC (Kunde *et al.*, 1974). After correcting for the difference between the two instrument functions, the IRIS radiances were found to be systematically lower than the SIRS measurements by as much as 4 ergs at 668.1 cm^{-1}, and by lesser amounts in the other channels. Of this 4 erg difference at 668.1 cm^{-1}, about 2 ergs can be attributed to the uncertainty in the IRIS instrument function, which has already been considered. There remains a possible 2 erg systematic error in the IRIS measurements due to calibration error.

In summary, the sum of the possible systematic errors in the calculated and in the measured radiance at 668.1 cm^{-1} is at most 8 ergs, with

a more likely value of 6 ergs. The average difference between the calculated and the measured radiances is, however, 12 ergs. Of this difference, 4 to 6 ergs remain unaccounted for, and the only remaining source of error seems to be the *in situ* profiles. From the R/NSC (1972) and Kunde *et al.* (1974), it appears that systematic errors in the rocketsonde measured temperatures of 5 to 10 K are quite possible.

Therefore, the results of this study indicate that systematic errors in the rocketsonde measurements exist. A rough estimate of the size of this error can be obtained from the radiance difference: a 4 to 6 erg error at 668.1 cm^{-1} translates roughly into a temperature error at 3.2 mb of 4 to 6 K. Since the systematic error probably increases with height, the error in the *in situ* temperature above 40 km is probably greater.

The fact that the *in situ* profiles contain systematic errors means that accurate verification of the retrieved profiles is impossible. Also, until the systematic errors in the measured and the calculated radiances are corrected, the retrieved profiles will be unreliable. Further research is needed, particularly to correct the absolute calibration of the IRIS and to determine the actual instrument function. However, if the errors in the calculated and the measured radiances are in the direction indicated, then the retrieved profiles probably set a lower limit on the actual profiles. And if further research shows that the radiance errors are less than indicated, the retrieved profiles may, in fact, be more accurate than the *in situ* profiles.

INVERSIONS WITH SYNTHETIC DATA

In order to investigate the accuracy and convergence properties of the retrieval process, the inversion routine was first applied to synthetic radiance data. Before presenting the results of this test, some comments on the temperature interpolation scheme and the best measure of the accuracy of the retrieved profiles are necessary.

The inversion routine relaxes the temperature at the three levels: z_1(3.2 mb $\sim$ 40 km); z_2(20.4 mb $\sim$ 27 km), and, z_3(60.0 mb $\sim$ 19 km). Between these levels, the temperature is found by linear interpolation in $z = -\ln(P/P_o)$. Below z_3, the temperature is merged with the *in situ* profile at 127 mb. There remains the problem of specifying the profile above z_1.

As mentioned before, the stratosphere during the period under investigation was relatively quiet. The level of the stratopause remained between 1.8 and 1.1 mb while the stratopause temperature varied over only 8 K. Above z_1, the individual profiles varied from the average profile with an average standard deviation at all levels of 2.5 K, and with a maximum standard deviation of 4.3 K at 1.8 mb. Therefore, for the profile above z_1 in the inversion routine, I decided to use a profile parallel to the average profile for the nine cases. The effect of this approximation on the accuracy of the retrieved profiles is demonstrated in the tests with synthetic data.

When evaluating the inversion process, there are several possible measures of the accuracy of the retrieved profiles. First, there is the

difference between the "exact" and the retrieved temperatures at the levels z_i--$\Delta\theta^{(n)}(z_i)$-- which measures the error in the retrieved profile only at the three specific points. Secondly, there is $\Delta\theta^{(n)}_{rms}$, the root mean square error integrated between z_1 and z_3, which measures the overall error in the retrieved profile between z_1 and z_2. Note, however, that even in these tests with error-free synthetic radiance data, neither $\Delta\theta^{(n)}(z_i)$, nor $\Delta\theta^{(n)}_{rms}$ can, in general approach zero exactly. The reason for this is that the synthetic radiance data are generated from the actual *in situ* profiles (here, the "exact" profiles). However, the retrieved profiles have only three degrees of freedom and cannot fit the fine structure of the "exact" profiles perfectly. The best fit, in the r.m.s. sense, between the "exact" and the retrieved profiles will, in general, produce errors at the levels z_i, while an exact fit at the levels z_i will necessarily produce a non-zero value for $\Delta\theta_{rms}$ (see Fig. 15).

However, if the "exact" and the retrieved temperatures, averaged over layers of significant thickness, are compared, the fine structure of the "exact" profile tends to be smoothed out and the agreement between the "exact" and the retrieved profiles should be improved. Therefore, the temperatures averaged over layers extending over approximately $z_i \pm 5$ km --$\bar{\theta}^{(n)}(z_i)$-- have been computed for both the exact and the retrieved profiles. Note that the layer-averaged temperatures $\bar{\theta}^{(n)}(z_i)$ are also more significant than the $\theta^{(n)}(z_i)$ for use in numerical weather prediction models, which will probably be a prime application of remote temperature sensing.

In these tests with synthetic data, the convergence characteristics

of the various measures of temperature error were examined to discover: 1) the accuracy of the retrieval process with and without random noise in the radiance data, and, 2) the criterion for stopping the iteration procedure.

The *in situ* temperature profiles for the nine cases were used to generate "exact" synthetic radiance data for the four channels whose weighting functions are shown in Fig. 10. These data were used as input to the inversion routine. At each iteration n, the following quantities were computed:

1) $\theta^{(n)}(z_i)$: the retrieved temperature at the levels z_i.

2) $\bar{\theta}^{(n)}(z_i)$: the retrieved temperatures averaged over approximately $z_i \pm 5$km.

3) $\Delta\theta^{(n)}_{rms}$: the r.m.s. difference between the "exact" and the retrieved profiles between the levels z_1 and z_3.

4) $R^{(n)}_{rms}$: the r.m.s. residuals for weighting functions 1, 2, and 3.

5) $R^{(n)}_4$: the residual for weighting function 4 (Fig. 10), which is not relaxed but sounds most of the stratosphere.

Each case was run using two initial guesses for $\theta(z)$:A, for which the initial guess is a reasonable approximation to the real profile, with $\theta^{(0)}(z_1) = 250$ K, $\theta^{(0)}(z_2) = 225$ K, and $\theta^{(0)}(z_3) = 215$ K; and B, for which the atmosphere between z_1 and z_3 is isothermal at 240 K. The relaxation procedure was iterated nine times.

Convergence of the retrieved profiles was obtained for all cases and

for both initial guesses. Fig. 11 shows $R^{(n)}_{rms}$ vs. n and Fig. 12 shows $\Delta\theta^{(n)}_{rms}$, for guess A. Figs. 13 and 14 shows the corresponding values for guess B. Understandably, guess A converges more rapidly than B. For guess A, $\Delta\theta^{(n)}_{rms}$ reaches a minimum for n between 1 and 4, and remains essentially constant thereafter. For guess B, the corresponding values of n range between 5 and 7. Note, however, that at the value of n for which $\Delta\theta^{(n)}_{rms}$ reaches a minimum, $R^{(n)}_{rms}$ may be as large as 1 percent and is still decreasing.

The question arises whether or not any improvement in the retrieved profile is obtained by continuing the iteration beyond the point where $\Delta\theta^{(n)}_{rms}$ reaches a minimum, so that $R^{(n)}_{rms}$ may be decreased further. Investigation shows that, for those values of n for which $\Delta\theta^{(n)}_{rms}$ remains constant, all other measures of the accuracy of the retrieved profile remain constant also. In particular, no decrease in the mean error in the layer-averaged temperatures is gained by continuing the iteration past the point at which $\Delta\theta^{(n)}_{rms}$ is a minimum. Therefore, $\Delta\theta^{(n)}_{rms}$ is a good overall indicator of the accuracy of the retrieved profile for different n.

The question remains then, why does the accuracy of the retrieved profile not improve beyond the point of minimum $\Delta\theta^{(n)}_{rms}$, even though the radiance data are exact and the $R^{(n)}_{rms}$ are decreasing? The answer is apparently that even though the radiance data are exact, the temperature data are not: the three-parameter retrieved profile cannot fit the "exact" profile perfectly, and the profile above 3.2 mb for the retrieved profile is only an approximation to the "exact" profile. These two effects represent a kind of "noise" in the data and reducing the $R^{(n)}_{rms}$ below the

level of this noise does not increase the accuracy of the retrieved profile.

As mentioned previously, Conrath and Revah (1972) have indicated that the critical value of $n = n'$ which produces the most accurate solution is obtained by halting the iteration at that point on the $R^{(n)}_{rms}$ curve where the curvature is the greatest. From Figs. 12 and 14, one can see that the point of minimum $\Delta\theta^{(n)}_{rms}$ occurs for an n which is 2 or 3 less than the n for the maximum curvature in the $R^{(n)}_{rms}$ curve. Therefore, the maximum curvature criterion is acceptable, but, for "exact" data anyway, it leads to an unnecessarily large value of n'. The question will be investigated again for noisy synthetic data.

Now consider the accuracy of the retrieved profiles. After convergence, $\Delta\theta^{(n)}_{rms}$ for guess A varies between 1.1 K and 1.9 K for the nine cases, with an average of 1.6 K. The corresponding values for B are essentially the same. Table 3 gives the "exact" and the retrieved temperatures $\theta(z_i)$ for guesses A and B, and their differences. The average difference between the "exact" and the retrieved temperatures for the three levels is 0.3 K for guesses A and 0.7 K for B. The individual differences are much larger, as shown by the standard deviations, which average 1.3 K for guess A and 1.4 K for B. The largest individual error is 3.8 K. Since the mean error averaged over the nine cases approaches zero, the standard deviations of the errors gives a better measure of the uncertainty to be expected in any single inversion than the average error. Fig. 13 shows the retrieved profile for a typical case (6/25), along with the "exact" profile and the initial guess A.

Table 4 gives the "exact" and the retrieved layer-averaged temperatures and their differences. The accuracy of the $\bar{\theta}(z_i)$'s is significantly better than that of the $\theta(z_i)$'s. The mean error averaged over the three levels remains small while the standard deviations are decreased by about half, to 0.6 K for guess A and 0.7 K for B. The maximum individual error in the layer-averaged temperature is 1.2 K.

Consider now the differences between the retrieved temperatures for the two initial guesses, shown in Table 3. These differences are, on the average, less than the differences between the "exact" temperature and either retrieved temperature. Furthermore, the temperatures retrieved using guess A are uniformly lower at z_1 than those retrieved by B, higher at z_2, and lower again at z_3. However, these differences are small, averaging 0.7 K for all three levels, with a maximum of 1.3 K. The differences between the layer-averaged temperatures retrieved by A and by B, shown in Table 4, show the same systematic trend, but are less, averaging 0.4 K, with a maximum of 0.8 K.

The previous test used exact synthetic data. To test the effect of measurement noise on the inversion process, a similar test was run with random errors added to the exact radiance. The random errors were generated from a normal distribution of mean zero and standard deviation of 0.5 ergs, approximating the noise of the IRIS-D. For each of the nine cases, inversions were run with six different sets of random noise, and using initial guesses A and B.

The results for a typical case, 6/25, will be shown in some detail. Fig. 16 shows the curve of $R^{(n)}_{rms}$ vs. n, while Fig. 17 shows $\Delta\theta^{(n)}_{rms}$ vs.

n, for initial guess A. Note that $\Delta\theta^{(n)}_{rms}$ goes to a minimum after 1 to 3 iterations, but may then increase. The point of maximum curvature on the $R^{(n)}_{rms}$ curve (as determined by eye), occurs for n equal to 1 or 2, while the rate of convergence of the residuals varies over a wide range. In these instances, the point of maximum curvature is the same as the point of minimum error in the retrieved profiles, so that the maximum curvature criterion is valid. Note the correlation, in these figures, between the size of the residuals and the accuracy of the retrieved profiles, as measured by $\Delta\theta^{(n)}_{rms}$.

Figs. 18 and 19 show the same curves for initial guess B. Note that, even for an isothermal guess, the $\Delta\theta^{(n)}_{rms}$ curve decreases to a minimum and diverges thereafter. Also, the point of maximum curvature occurs for n 1 to 3 greater than the point of minimum $\Delta\theta^{(n)}_{rms}$. In this case, using the maximum curvature criterion increases the error in the retrieved profiles over the minimum possible error. Table 5 gives the values of $\Delta\theta^{(n)}_{rms}$ and $R^{(n)}_{rms}$ for the two criteria: n_1'--the minimum $\Delta\theta^{(n)}_{rms}$, and n_2'--the maximum curvature. The total r.m.s. error in the radiances is also given. For guess A, n_1' equals n_2', so the accuracy of the retrieved profiles is the same in both cases. For guess B, n_2' is greater than n_1' by from 1 to 3. The total average decrease in accuracy, judged by the average $\Delta\theta^{(n)}_{rms}$, resulting from using the maximum curvature criterion, is quite small: only 0.1 K. In individual cases, however, such as 5 and 6 with guess B, the increased error is from .4 to .6 K.

Note that the correlation between the r.m.s. noise and $\Delta\theta^{(n)}_{rms}$ is weak. Cases 3 and 6 have the same level of noise but differ in $\Delta\theta^{(n)}_{rms}$

by 0.5 K, while case 2 has greater noise than case 6, but a lower $\Delta\theta^{(n)}_{rms}$ by 0.5 K. Also, $R^{(n)}_{rms}$ is not a consistent indicator of the r.m.s. noise: case 2 has a relatively large level of noise but a relatively small value of $R^{(n)}_{rms}$ at convergence.

Table 6 shows the same statistics as Table 5, but for 6/8, and in general, implies the same results. In particular, the value of n at maximum curvature is 1 or 2 greater than the n for the minimum $\Delta\theta^{(n)}_{rms}$. The increase in $\Delta\theta^{(n)}_{rms}$ due to using the maximum curvature criterion is again, small: only about 0.2 K for both guess A and B. Also, guess A gives a retrieved profile only slightly better than guess B. Note also that the average $R^{(n)}_{rms}$ at convergence for 6/8 is about twice that for 6/25, although they both have about the same retrieved accuracy.

In summary, these results show that using the point of maximum curvature on the $R^{(n)}_{rms}$ curve as the convergence criterion is, in general, valid, although slightly better results are obtained in some cases from one less iteration. They also show that the accuracy of the retrieved profile is practically independent of the initial guess.

Consider now the level of accuracy of the retrieved profile in the presence of noise. From all these tests with noisy synthetic data and for both initial guesses, the average value of $\Delta\theta^{(n)}_{rms}$ is 2.0 K, using the maximum curvature criterion, compared to an average of 1.6 K without noise. The uncertainty in the layer-averaged temperature (perhaps a more useful measure of the retrieved accuracy than $\Delta\theta^{(n)}_{rms}$) is about 1.1 K for guess A compared to 0.6 K for the case with no noise. For guess B, the uncertainty in $\bar{\theta}(z_i)$ is 1.2 K compared to 0.7 K without noise. An individual error of

3.0 K was observed, but this error was due to an unusually large (and statistically improbable) value of the noise.

The average of R_4 for these tests with noise is 0.7 percent for guess A, with a maximum of 1.6 percent, and 0.5 percent for B, with a maximum of 1.5 percent.

INVERSIONS WITH REAL DATA

The results of the inversions of the IRIS data are shown in Figs. 20 and 21, and in Tables 7 and 8. Fig. 20, shows $R^{(n)}_{rms}$ vs. n using initial guess A. Convergence is obtained in all cases, and the critical value n′ for which the curvature is greatest varies between 1 and 3. Note that initial guess A is closer to the final retrieved profiles with real data than it is to the "exact" profiles using synthetic data, so that the residuals for n = 0 are relatively small. The values of the $R^{(n)}_{rms}$'s are comparable to those obtained from the tests with 1 percent random noise. Therefore, the reported level of random noise for the IRIS-D of about 1 percent (Hanel *et al.*, 1972) tends to be confirmed, or at least, not contradicted. Systematic errors in the radiance data however, would not necessarily be reflected in the $R^{(n)}_{rms}$ curves. Due to the probable systematic errors in the *in situ* profiles, the curves of $\Delta\theta^{(n)}_{rms}$ cannot be used to judge the accuracy of the retrieved profiles, and so they are not shown here. The average value of $\Delta\theta^{(n)}_{rms}$ at convergence is 7.9 K.

Table 7 lists the retrieved and the *in situ* temperatures $\theta(z_i)$, along with their differences. The differences are systematic and increasing with height. At z_1, the mean difference is 11.5 K with a standard deviation of ±2.2 K; at z_2, 6.0 ± 3.7 K; and at z_3, 3.1 ± 1.9 K. Table 8 shows the differences between the retrieved and measured layer-averaged temperatures, $\bar{\theta}(z_i)$, which are quite similar. The mean differences are: at z_1, 10.3 ± 2.8 K; at z_2, 6.6 ± 2.9 K; and at z_3, 2.7 ± 1.7 K.

The profiles retrieved using initial guess B show essentially the same characteristics as those retrieved using A. For each day, $R^{(n)}_{rms}$ converges to approximately the same value, although the critical value n' varies between 5 and 7. The average values of $\Delta\theta^{(n)}_{rms}$ and $R^{(n)}_{4}$ are within 0.02 K and 0.003 of their previous values. The mean differences and the standard deviations between the temperatures retrieved using A minus those using B are: -0.2 ± 0.5 K at z_1, $+1.2 \pm 1.3$ K at z_2, and -2.0 ± 1.0 K at z_3. Since the tests with synthetic data show that guess A gives slightly better results than B, all further discussion will use the results from A.

Fig. 21a-i show the retrieved and the measured profiles for the nine cases. Note that the two profiles merge at 127 mb, and that above 3.2 mb, the retrieved profile is parallel to the average *in situ* profile for the nine cases. The systematic difference between the retrieved and the *in situ* profiles is clearly visible in these figures. Note also that the day-to-day variation among the retrieved profiles is less than that among the measured profiles.

Because of the systematic difference between the retrieved and the *in situ* profiles, there is little point in discussing whether or not the inverted profiles can retrieve structural details in the measured profiles. In any case, because of the limited vertical resolution of the retrieved profiles, details with a scale smaller than about 10 km cannot be retrieved, while details with a scale greater than 10 km usually have small amplitude in these particular profiles.

The sources of the systematic differences between the IRIS measurements

and the *in situ* measurements have already been considered with respect to the direct problem. From the comparison of the measured and the calculated radiances, even after corrections for the possible systematic errors in the measured and the calculated radiances were made, it was concluded that the *in situ* measurements probably contain systematic errors. It should be possible to show the same conclusion from the differences between the retrieved and the *in situ* profiles, by incorporating the possible systematic corrections into the inversion routine. However, such a demonstration using the retrieved profiles is more difficult because of the interactions between the retrieved temperatures at the various levels. For example, overcorrection in the radiance for one channel would lead to a retrieved temperature at the corresponding level which is too high. In response, the retrieved temperatures at the other levels, due to this effect, would be too low. Therefore, greater care in applying the corrections to the measured and the calculated radiances is needed when considering the retrieved temperatures than when considering the direct problem.

With these comments in mind, inversions were run using the real data, with rough corrections made for the possible systematic errors in the measured and the calculated radiances. These corrections amounted to adding 5 ergs to the measured radiances to correct for the combined effects of the IRIS calibration error, the error in the instrument function, and the errors in the transmission function. This value for the correction applies actually only to the radiance at 668.1 cm^{-1} as estimated in the section on the direct problem: for the other radiances, it is probably too much. A value of 200 K was used for $\theta(z_T)$ to allow for the uncertainty

in this temperature. Note that all the corrections were made in such a way as to minimize the difference between the retrieved and the *in situ* profiles.

The effect of these corrections was to raise both the temperatures $\theta(z_i)$ and $\bar{\theta}(z_i)$ by 5.7 ± 0.3 K evenly at all three levels. Consider now the average discrepancy between the retrieved and the *in situ* profiles shown in Tables 7 and 8. Adding the radiance corrections overcompensates by about 3 K for the discrepancy at z_3, while it effectively eliminates the discrepancy at z_2. However, there remains an average difference between the retrieved and the *in situ* temperatures of about 6 K in $\theta(z_1)$ and about 4.5 K in $\bar{\theta}(z_1)$. Adding the radiance corrections also reduces $\Delta\theta_{rms}$ from 7.9 K to 3.9 K.

Clearly these corrections for the possible systematic errors are crude. However, the systematic difference between the retrieved and the measured profiles, even with these corrections applied, still indicates a systematic error in the *in situ* temperature measurements of about 4 to 6 K at 40 km.

As the situation stands, the uncertainty in the retrieved profiles is half or more of the difference between the retrieved and the *in situ* profiles. While the remaining difference still indicates the presence of a systematic error in the *in situ* measurements, the magnitude of this error is poorly known. Further research into the sources of the possible errors in the calculated and the measured radiances would be useful, both in reducing the errors in the retrieved profiles, and in specifying more accurately the error in the *in situ* measurements. The most important areas for further work are in:

1) determining the actual IRIS-D instrument function, both apodized and unapodized;
2) evaluating the calibration error in the IRIS-D, and,
3) extending the transmission calculations to above 58 km to reduce the uncertainty due to $\theta(z_T)$.

If these three areas of uncertainty can be significantly reduced, greater confidence can be placed in both the retrieved profiles and the error in the *in situ* measurements.

Finally, the discrepancy in the value of R_4 must be accounted for. With only random noise in the data, the average value of R_4 should be of the order of the measurement noise: in the tests of synthetic radiance data with 1 percent noise, the average R_4 was 0.5 percent. From the inversions with real data, R_4 averaged 3.1 ± 1.1 percent. This discrepancy is not surprising, however, in view of the possible systematic errors in the radiance data of up to 10 percent and the errors in the *in situ* measurements, which affect the assumed profile above 3.2 mb. The large value of R_4 therefore, merely indicates the presence of systematic errors without indicating their source.

CONCLUSION

The goal of this research has been to obtain remote temperature soundings up to 3.2 mb using the unapodized radiance data from the IRIS-D. For this purpose, a set of three weighting functions which peak in the stratosphere has been found. In order to obtain retrieved temperatures using this limited set of weighting functions, supplementary *in situ* measurements of the tropospheric temperatures are used. Tests with synthetic radiance data show that retrieved temperatures can be obtained in the stratosphere with a vertical resolution of about 10 km and an uncertainty due to random instrument noise of 1.1 K.

However, there are several sources of systematic error in the data which must be corrected for before the profiles retrieved from actual radiance data can be used with confidence. These errors include: uncertainty in the actual IRIS-D instrument function, possible errors in the absolute calibration of the IRIS-D, and uncertainties in the transmission functions above 58 km. These errors may cause the retrieved profiles to be systematically low by as much as 6 to 8 K at 40 km.

In spite of these uncertainties, the results strongly suggest a systematic error in the *in situ* measurements of at least 4 to 6 K at 40 km. Unfortunately, these errors make an accurate verification of the retrieved profiles impossible. Until the necessary corrections to the data can be made, the retrieved temperatures and the *in situ* temperatures will be incompatible. At present, both systems of temperature measurement appear

to contain systematic errors, but it is not yet clear which system is the more accurate.

LIST OF REFERENCES

Chahine, M. T., 1968: Determination of the temperature profile in an atmosphere from its outgoing radiance. *J. Opt. Soc. Amer.*, 58, 1634-1637.

_____ , 1970: Inverse problems in radiative transfer: determination of atmospheric parameters. *J. Atmos. Sci.*, 27, 960-967.

_____ , 1972: A general relaxation method for inverse solution of the full radiative transfer equation. *J. Atmos. Sci.*, 29, 741-747.

Conrath, B. J., 1972: Vertical resolution of temperature profiles obtained from remote radiation measurements. *J. Atmos. Sci.*, 29, 1262-1271.

Conrath, B. J., and I. Revah, 1972: A review of nonstatistical techniques for the estimation of vertical atmospheric structure from remote infrared measurements, in *Mathematics of Profile Inversion*, ed. L. Colin, NASA TM X-62, 150, pp. 1-36; 1-49.

Hanel, R. A., B. Schlachman, D. Rogers, and D. Vanous, 1971: Nimbus 4 Michelson Interferometer. *Applied Optics*, 10, 1376-1382.

Hanel, R. A., B. J. Conrath, V. G. Kunde, C. Prabhakara, I. Revah, V. V. Salomonson, and G. Wolford, 1972: The Nimbus 4 infrared spectroscopy experiment: 1. Calibrated thermal emission spectra. *J. Geophys. Res.*, 77, 2629-2641.

Kunde, V. G., B. J. Conrath, R. A. Hanel, W. C. Maguire, C. Prabhakara, V. V. Salomonson, 1974: The Nimbus 4 infrared spectroscopy

experiment: 2. Comparison of observed and theoretical radiances from 425-1450 cm^{-1}. *J. Geophys. Res.*, 79, 777-784.

Kunde, V. G., and W. C. Maguire, 1974: Direct integration transmittance model. *J. Quant. Spectrosc. Radiat. Transfer*, 14, 803-817.

Rocket/Nimbus Sounder Comparison (RNSC), 1972, NASA SP-296.

U.S. Standard Atmosphere, 1962: Washington, D.C., Government Printing Office.

Westwater, E. R., and O. N. Strand, 1972: Inversion techniques, in *Remote Sensing of the Troposphere*, ed. V. E. Derr (NOAA, Boulder, Colorado), pp. 16-1; 16-13.

Table 1.--The residuals $R_j(\tilde{\nu}_i)$ for a 2 K perturbation of the temperature profile $\theta(z_j)$ in the j'th 2 km thick layer*

(×1000)

Layer			$\tilde{\nu}_i$ (cm^{-1})									
j	Center (mb)	Height (km)	668.1 (1)	648.6 (2)	667.4 (3)	654.9 (4)	645.1 (5)	639.9 (6)	629.8 (7)	625.0 (8)	610.0 (9)	599.9 (10)
1	0.31	59	2.17	0.58	1.45	0.20	0.17	0.16	0.07	0.04	0.01	0.01
2	0.40	57	1.01	0.51	0.66	0.14	0.10	0.09	0.07	0.04	0.01	0.01
3	0.52	55	0.97	0.44	0.65	0.14	0.12	0.10	0.06	0.04	0.01	0.01
4	0.66	53	1.12	0.38	0.77	0.15	0.14	0.11	0.05	0.04	0.01	0.01
5	0.86	51	1.35	0.36	0.93	0.17	0.16	0.12	0.04	0.04	0.01	0.01
6	1.11	49	1.62	0.38	1.11	0.20	0.18	0.14	0.04	0.04	0.01	0.01
7	1.42	47	1.94	0.46	1.32	0.24	0.21	0.16	0.05	0.04	0.01	0.01
8	1.82	45	2.29	0.57	1.56	0.30	0.25	0.19	0.06	0.04	0.01	0.01
9	2.34	43	2.59	0.70	1.76	0.38	0.29	0.23	0.08	0.04	0.02	0.01
10	3.01	41	2.73	0.87	1.85	0.47	0.35	0.27	0.11	0.05	0.02	0.01
11	3.89	39	2.72	1.11	1.85	0.60	0.43	0.33	0.14	0.06	0.03	0.01
12	5.06	37	2.51	1.41	1.74	0.78	0.54	0.43	0.18	0.08	0.04	0.02
13	6.63	35	2.16	1.73	1.61	1.00	0.69	0.55	0.23	0.11	0.05	0.02
14	8.73	33	1.80	2.00	1.55	1.28	0.88	0.70	0.29	0.14	0.06	0.03
15	11.5	31	1.49	2.20	1.59	1.59	1.11	0.88	0.36	0.19	0.08	0.04
16	15.3	29	1.16	2.44	1.70	2.00	1.41	1.12	0.45	0.24	0.10	0.05
17	20.4	27	0.77	2.62	1.84	2.55	1.77	1.41	0.57	0.30	0.12	0.06
18	27.3	25	0.34	2.61	1.94	3.15	2.21	1.78	0.73	0.38	0.16	0.08
19	36.7	23	-.07	2.45	1.95	3.74	2.72	2.22	0.94	0.49	0.21	0.10
20	49.6	21	-.39	2.33	1.79	4.20	3.27	2.73	1.19	0.62	0.27	0.13
21	67.5	19	-.51	2.31	1.41	4.35	3.79	3.26	1.47	0.77	0.33	0.16
22	92.3	17	-.34	2.23	0.86	4.01	4.14	3.75	1.80	0.95	0.41	0.20
23	127	15	-.05	1.87	0.33	3.00	4.20	4.19	2.30	1.24	0.56	0.27
24	175	13	0.07	1.13	0.06	1.49	3.68	4.30	3.09	1.73	0.81	0.40
25	240	11	0.05	0.37	0.01	0.40	2.60	3.88	4.45	2.71	1.35	0.69
26	322	9	0.03	-.02	0.00	0.04	1.16	2.44	5.54	3.97	2.20	1.18
27	425	7	0.03	-.07		0.00	0.25	0.86	5.01	4.80	3.21	1.80
28	552	5	0.02	-.03			0.02	0.13	2.83	4.52	4.02	2.47
29	709	3	0.01	0.03			0.00	0.01	0.86	3.25	4.25	3.03
30	900	1	0.00	0.05				0.00	0.11	1.76	3.62	3.32

*The wavenumbers $\tilde{\nu}_i$ refer to the weighting functions shown in Fig. 7. The anomalous behavior of layer 1 is explained in Appendix B. The residuals below 322 mb are unreliable, since the absorption due to water vapor has not been taken into account in the transmission functions.

Table 2.--The calculated and the measured radiances and their differences for nine cases taken from the R/NSC
(in ergs)

	$\tilde{\nu}_i$ (cm^{-1})											
	668.1 (1)			648.6 (2)			654.9 (3)			667.4 (4)		
	Calc.	Meas.	Diff.	Calc.	Meas.	Diff.	Calc.	Meas.	Diff.	Calc.	Meas.	Diff.
6/8	85.8	74.8	11.0	58.7	53.7	5.0	50.6	48.0	2.7	68.3	63.4	4.9
6/15	79.8	72.8	7.0	56.9	54.4	2.5	49.7	48.2	1.5	65.2	61.5	3.7
6/17	87.2	72.5	14.8	61.2	53.3	8.0	53.1	47.6	5.6	71.1	62.0	9.0
6/22	81.8	73.2	8.7	58.2	54.8	3.4	50.8	49.0	1.9	66.7	62.2	4.5
6/25	85.4	73.5	12.0	61.3	54.8	6.5	53.8	49.0	4.8	70.3	64.4	5.9
7/1	86.4	71.5	14.9	61.5	52.3	9.2	53.6	47.4	6.2	70.6	61.5	9.1
7/2	82.0	71.5	10.6	57.1	53.7	3.4	49.3	46.4	2.9	66.3	61.1	5.2
7/6	85.9	71.9	14.0	62.4	54.0	8.4	54.8	49.4	5.4	70.7	62.3	8.4
7/13	85.6	71.4	14.3	59.5	52.3	7.3	51.3	47.1	4.2	69.0	61.4	7.7
Mean	84.4	72.6	11.9	59.6	53.7	6.0	51.9	48.0	3.9	68.7	62.2	6.5
Std. Dev.	2.4	1.1	2.7	1.9	0.9	2.3	1.9	0.9	1.6	2.1	1.0	1.9

Table 3.--The "exact" and the retrieved temperatures $\theta(z_i)$ and their differences for inversions of error-free synthetic radiance data*
(in K)

			$\theta(z_1)$					$\theta(z_2)$					$\theta(z_3)$				
	n'_A	n'_B	θ_E	Δ_{E-A}	θ_A	Δ_{E-B}	θ_B	θ_E	Δ_{E-A}	θ_A	Δ_{E-B}	θ_B	θ_E	Δ_{E-A}	θ_A	Δ_{E-B}	θ_B
6/8	5	7	260.6	-0.5	261.1	-1.8	262.4	223.5	-2.5	226.0	-1.6	225.1	215.8	2.4	213.4	1.3	214.5
6/15	4	7	257.2	1.3	255.9	1.1	256.1	227.0	0.4	226.6	1.3	225.7	216.4	0.8	215.6	-0.2	216.6
6/17	2	7	262.3	0.1	262.2	-0.3	262.6	234.3	2.7	231.6	3.8	230.5	219.0	-0.9	219.9	-1.8	220.8
6/22	4	7	259.8	2.1	257.7	1.9	257.9	226.0	-1.7	227.7	-1.0	227.0	217.3	0.9	216.4	-0.1	217.4
6/25	2	7	261.6	1.1	260.5	0.8	260.8	232.4	0.9	231.5	1.8	230.6	220.4	0.1	220.3	-1.3	221.7
7/1	2	8	259.8	-1.7	261.5	-2.0	261.8	231.7	0.3	231.4	1.0	230.7	219.0	-0.5	219.5	-0.9	219.9
7/2	4	7	258.6	1.0	257.6	0.5	258.1	227.2	-0.6	227.8	0.6	226.6	213.9	-2.5	216.4	-2.7	216.6
7/6	2	7	260.8	-0.2	261.0	-0.4	261.2	233.1	1.3	231.8	1.9	231.2	219.7	-0.5	220.2	-1.7	221.4
7/13	3	8	263.3	2.1	261.2	1.8	261.5	230.5	1.4	229.1	2.4	228.1	215.8	-1.0	216.8	-1.3	217.1
Mean				0.6		0.2			0.2		1.1			-0.1		-0.9	
Std. dev.				1.2		1.3			1.5		1.6			1.3		1.1	

*The critical value n' is the order of iteration for which the curvature of the R_{rms} curve is a maximum. E refers to the "exact" profile while A and B refer to the profiles retrieved using initial guesses A and B respectively.

Table 4.--The "exact" and the retrieved layer-averaged temperatures $\bar{\theta}(z_i)$ and their differences for inversions of error-free synthetic data
(in K)

			$\bar{\theta}(z_1)$					$\bar{\theta}(z_2)$					$\bar{\theta}(z_3)$				
	n'_A	n'_B	$\bar{\theta}_E$	Δ_{E-A}	$\bar{\theta}_A$	Δ_{E-B}	$\bar{\theta}_B$	$\bar{\theta}_E$	Δ_{E-A}	$\bar{\theta}_A$	Δ_{E-B}	$\bar{\theta}_B$	$\bar{\theta}_E$	Δ_{E-A}	$\bar{\theta}_A$	Δ_{E-B}	$\bar{\theta}_B$
6/8	5	7	259.8	-0.5	260.3	-0.6	260.4	231.4	-0.6	232.0	0.0	231.4	215.9	0.3	215.6	-0.2	216.1
6/15	4	7	252.9	-2.0	254.9	-2.1	255.0	231.2	-0.2	231.4	0.4	230.8	216.5	0.4	216.1	-0.2	216.7
6/17	2	7	261.2	0.2	261.0	-0.1	261.3	236.8	0.2	236.6	0.9	235.9	218.6	-0.8	219.4	-1.2	219.8
6/22	4	7	257.1	0.5	256.6	0.4	256.7	231.5	-1.1	232.6	-0.6	232.1	217.3	0.3	217.0	-0.3	217.6
6/25	2	7	259.7	0.1	259.6	0.0	259.7	236.2	-0.1	236.3	0.5	235.7	220.4	0.1	220.3	0.7	221.1
7/1	2	7	260.8	0.4	260.4	0.2	260.6	236.8	0.5	236.3	0.9	235.9	219.2	-0.7	219.9	-1.0	220.2
7/2	4	7	255.7	-1.0	256.7	-1.1	256.8	233.0	0.6	232.4	1.1	231.9	214.6	-0.7	215.3	-1.1	215.7
7/6	2	7	259.8	-0.2	260.0	-0.3	260.1	236.9	0.3	236.6	0.7	236.2	220.5	-0.4	220.9	-1.0	221.5
7/13	3	8	260.0	0.2	259.8	0.0	260.0	234.7	0.3	234.4	1.0	233.7	216.3	-1.0	217.3	-1.0	217.3
Mean				-0.3		-0.4			0.0		0.5			-0.3		-0.5	
Std. dev.				0.8		0.7			0.5		0.5			0.5		0.7	

Table 5.--The results of inversions of the synthetic radiance data for 6/25 with six sets of 1 percent random noise*

	Initial guess A						Initial guess B					
Total Error (%)	n_1'	$\Delta\theta_{rms}$ (K)	R_{rms} (%)	n_2'	$\Delta\theta_{rms}$ (K)	R_{rms} (%)	n_1'	$\Delta\theta_{rms}$ (K)	R_{rms} (%)	n'_2	$\Delta\theta_{rms}$ (K)	R_{rms} (%)
0.10	3	1.79	0.1	3	1.80	0.1	7	1.79	0.3	7	1.79	0.3
1.06	3	1.94	0.3	3	1.94	0.3	5	1.76	0.7	7	1.85	0.5
0.67	3	1.93	0.2	3	1.93	0.2	6	1.81	1.5	7	1.83	0.4
0.87	3	2.16	0.8	3	2.16	0.8	5	2.09	3.0	6	2.17	1.1
1.40	2	2.55	1.6	2	2.55	1.6	4	2.16	2.6	6	2.78	1.5
0.67	3	2.42	0.8	2	2.52	1.1	4	1.92	1.6	7	2.51	0.8
Mean		2.10	0.6		2.10	0.7		1.92	1.6		2.20	0.8
No Error	4	1.80	0.1	3	1.80	0.1	6	1.79	0.6	8	1.79	0.2

*The critical value n_1' is the order of iteration for the minimum $\Delta\theta_{rms}$ while n'_2 is the order of iteration at the point of maximum curvature of the R_{rms} curve.

Table 6.--The results of inversions of the synthetic radiance data for 6/8 with six sets of 1 percent random noise

	Initial guess A						Initial guess B					
Total Error (%)	n_1'	Θ_{rms} (K)	R_{rms} (%)	n_2'	Θ_{rms} (K)	R_{rms} (%)	n'_1	Θ_{rms} (K)	R_{rms} (%)	n_2'	Θ_{rms} (K)	R_{rms} (%)
0.78	4	1.68	1.6	6	1.68	1.1	6	1.50	1.1	6	1.50	1.1
1.25	2	2.20	3.3	4	2.54	1.9	5	2.62	2.5	6	2.87	1.8
0.52	3	2.09	2.4	4	2.40	1.8	5	2.45	2.5	6	2.72	1.8
0.62	3	1.88	2.0	5	2.27	1.1	5	2.02	2.2	6	2.11	1.5
1.17	4	1.82	1.0	4	1.82	1.0	6	1.68	1.1	7	1.73	0.7
1.60	3	2.16	2.3	4	2.45	1.8	5	2.61	2.5	6	2.83	1.9
Mean		1.97	2.0		2.19	1.5		2.15	2.0		2.29	1.5
No Error	5	1.34	0.4	6	1.34	0.2	7	1.22	0.5	8	1.23	0.3

Table 7.--The retrieved and the in situ temperatures $\Theta(z_i)$ and their differences for the inversion of the actual IRIS data using initial guess A* (in K)

		z_1 (3.2 mb)			z_2 (20.4 mb)			z_3 (60.0 mb)		
	n'	In Situ	Retrieved	Diff.	In Situ	Retrieved	Diff.	In Situ	Retrieved	Diff.
6/8	4	260.6	251.5	9.1	223.5	221.9	1.6	215.8	212.9	2.9
6/15	2	257.2	249.0	8.2	227.0	224.7	2.3	216.4	214.8	1.6
6/17	2	262.3	248.6	13.7	234.3	223.8	10.5	219.0	214.4	4.6
6/22	4	259.8	249.1	10.7	226.0	225.1	0.9	217.3	215.9	1.4
6/25	3	261.6	249.5	12.1	232.4	224.9	7.5	220.4	215.5	4.9
7/1	3	259.8	247.9	11.9	231.7	221.5	10.2	219.0	213.4	5.6
7/2	2	258.6	247.7	10.9	227.2	224.7	2.5	213.9	213.9	0.0
7/6	2	260.8	248.2	12.6	233.1	223.4	9.7	219.7	214.7	5.0
7/13	3	263.3	247.7	15.6	230.5	221.9	8.6	215.8	213.9	1.9
Mean				11.5			6.0			3.1
Std. dev.				2.2			3.7			1.9

*The critical value n' refers to the point of maximum curvature on the R_{rms} curve.

Table 8.--The retrieved and the in situ layer-averaged temperatures $\bar{\theta}(z_i)$ and their differences for inversions of the actual IRIS data using guess A (in K)

		z_1 (3.2 mb)			z_2 (20.4 mb)			z_3 (60.0 mb)		
	n'	In Situ	Retrieved	Diff.	In Situ	Retrieved	Diff.	In Situ	Retrieved	Diff.
6/8	4	259.8	250.4	9.4	231.4	226.8	4.6	215.9	214.5	1.4
6/15	2	252.9	248.6	4.3	231.2	228.6	2.6	216.5	215.3	1.2
6/17	2	261.2	248.2	13.0	236.8	227.8	9.0	218.6	214.5	4.1
6/22	4	257.1	248.8	8.3	231.5	229.0	2.5	217.3	216.2	1.1
6/25	3	259.7	249.1	10.6	236.2	229.0	7.2	220.4	216.1	4.3
7/1	3	260.8	247.3	13.5	236.8	225.9	10.9	219.2	214.3	4.9
7/2	2	255.7	247.5	8.2	233.0	228.4	4.6	214.6	213.6	1.0
7/6	2	259.8	247.7	12.1	236.9	227.5	9.4	220.5	215.9	4.6
7/13	3	260.0	247.1	12.9	234.7	226.2	8.5	216.3	214.2	2.1
Mean				10.3			6.6			2.7
Std. dev.				2.8			2.9			1.7

Fig. 1. The function $d\bar{T}/dz$ vs. z for $\bar{T} = \exp(-cP)$. $\bar{T}$ is the idealized average transmission along a vertical path from ∞ to the level z for a gas of constant composition, with pressure broadened, randomly distributed lines whose intensities and half widths do not depend upon temperature.

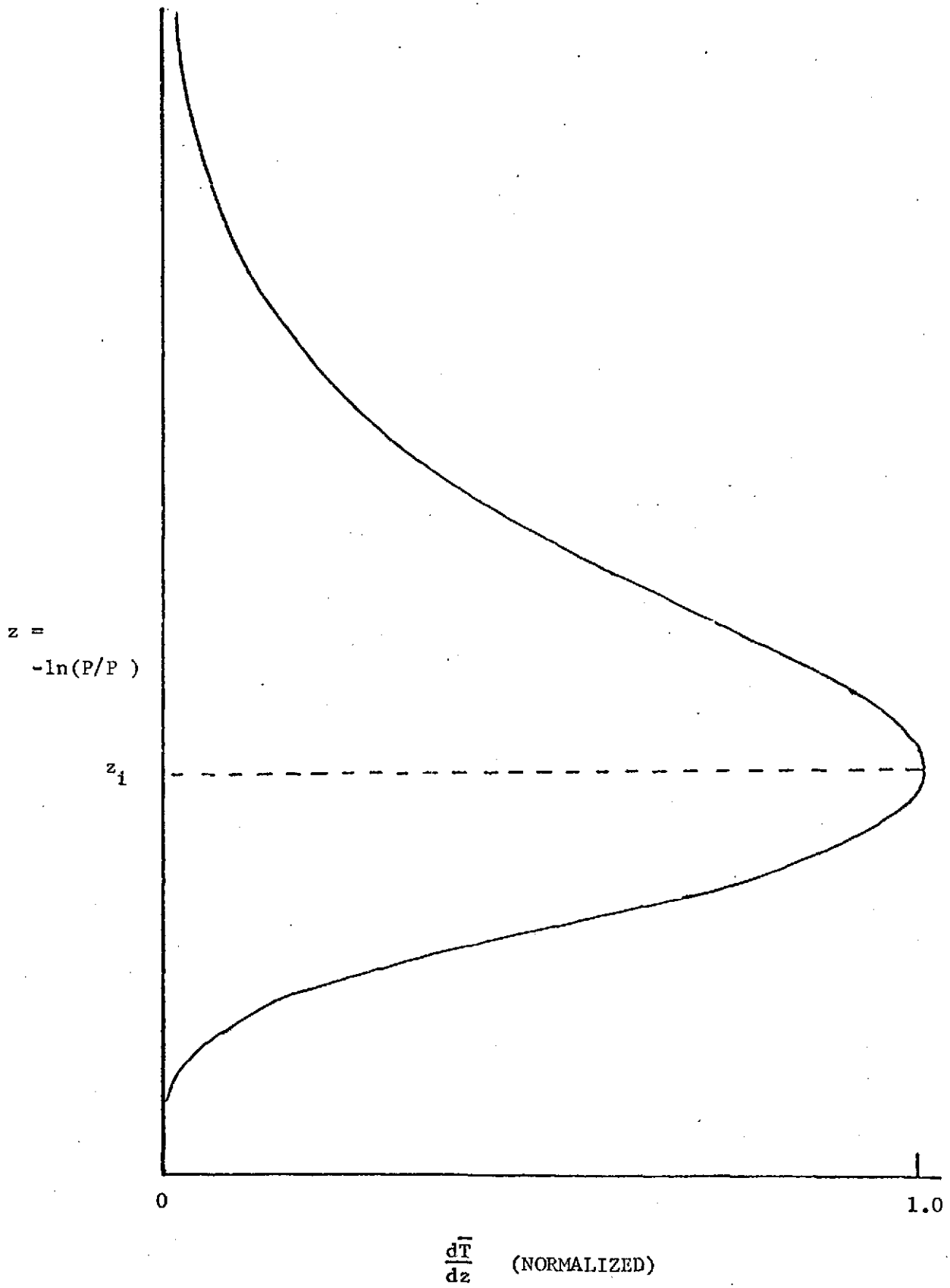
z =
-ln(P/P)
z_i
0
1.0
dT̄/dz (NORMALIZED)

Fig. 2. Weighting functions for the 15μ CO_2 band for an instrument function of resolution 2.8 cm^{-1}, from Conrath (1972).

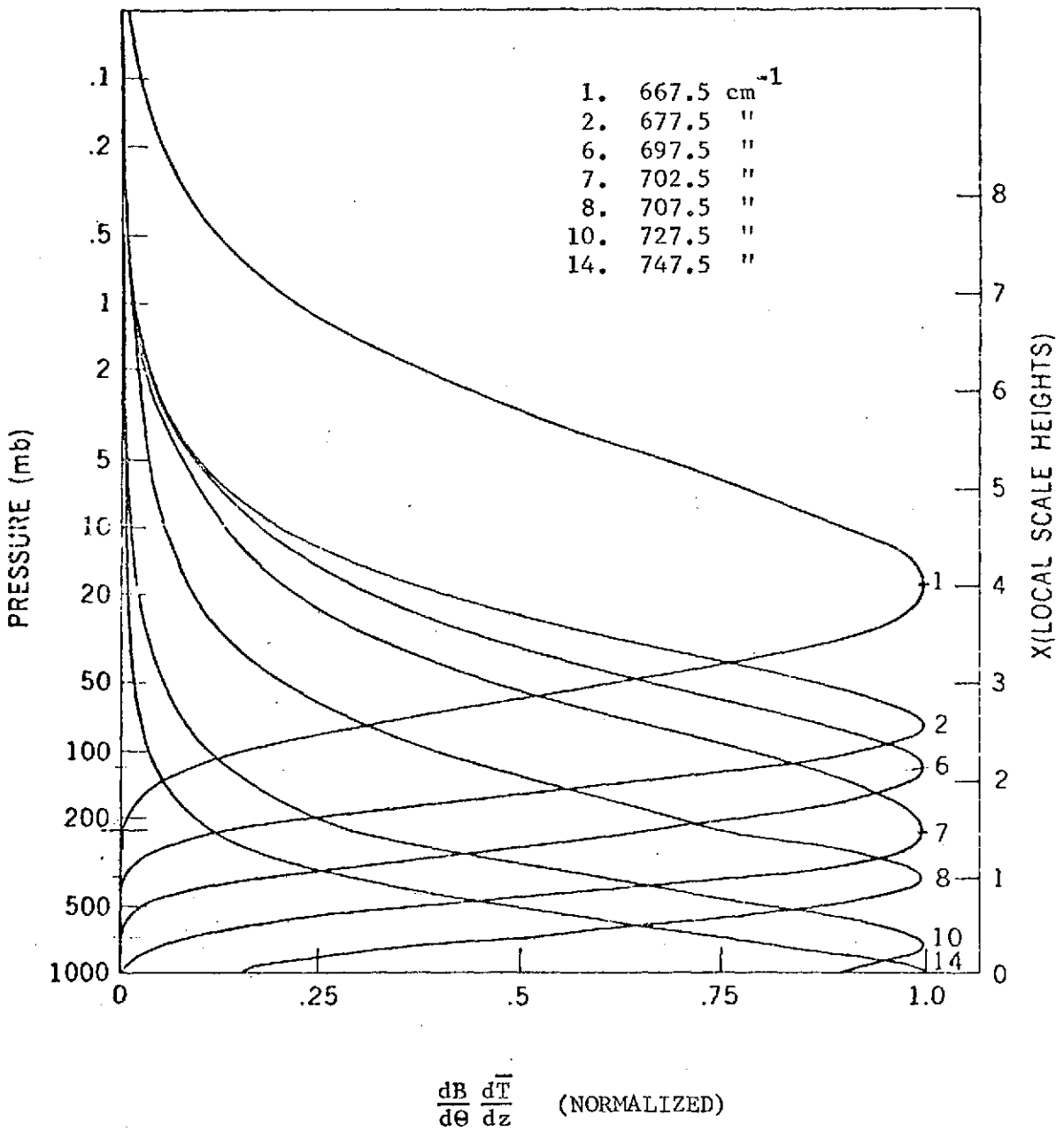
1. 667.5 cm-1
2. 677.5 "
6. 697.5 "
7. 702.5 "
8. 707.5 "
10. 727.5 "
14. 747.5 "
PRESSURE (mb)
.1
.2
.5
1
2
5
10
20
50
100
200
500
1000
0
.25
.5
.75
1.0
X(LOCAL SCALE HEIGHTS)
8
7
6
5
4
3
2
1
0
1
2
6
7
8
10
14
dB/dθ dT̄/dz (NORMALIZED)

Fig. 3. The υ_2 band of CO_2: the positions and relative intensities of the lines of the Q branch plus a few lines from the P and R branches.

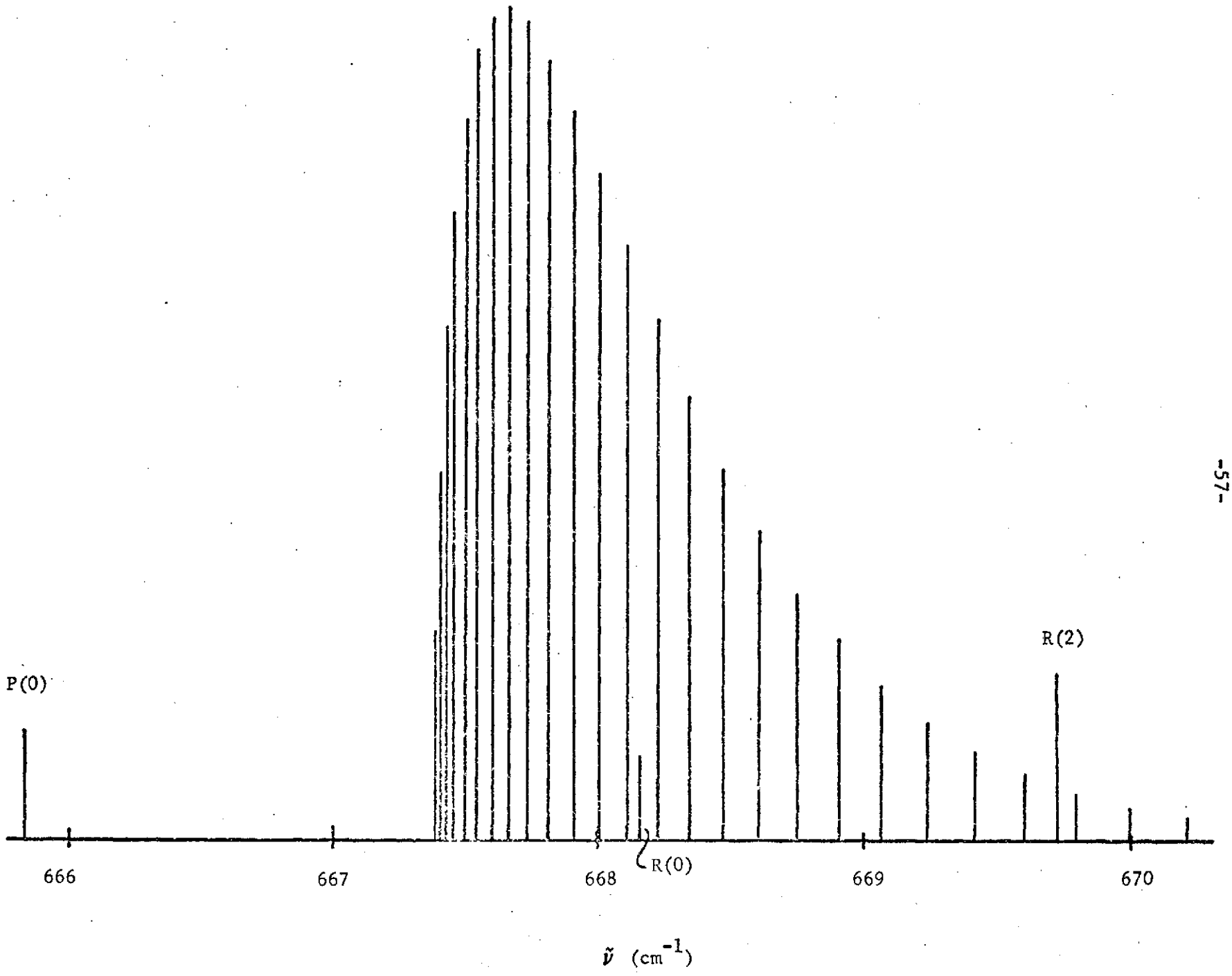
P(0)
R(2)
R(0)
666
667
668
669
670
$\tilde{\nu}$ (cm^{-1})

Fig. 4. The SIRS-A weighting functions $d\bar{T}/dz$, without the factor $dB/d\theta$, for a spectral resolution of 5 cm^{-1}.

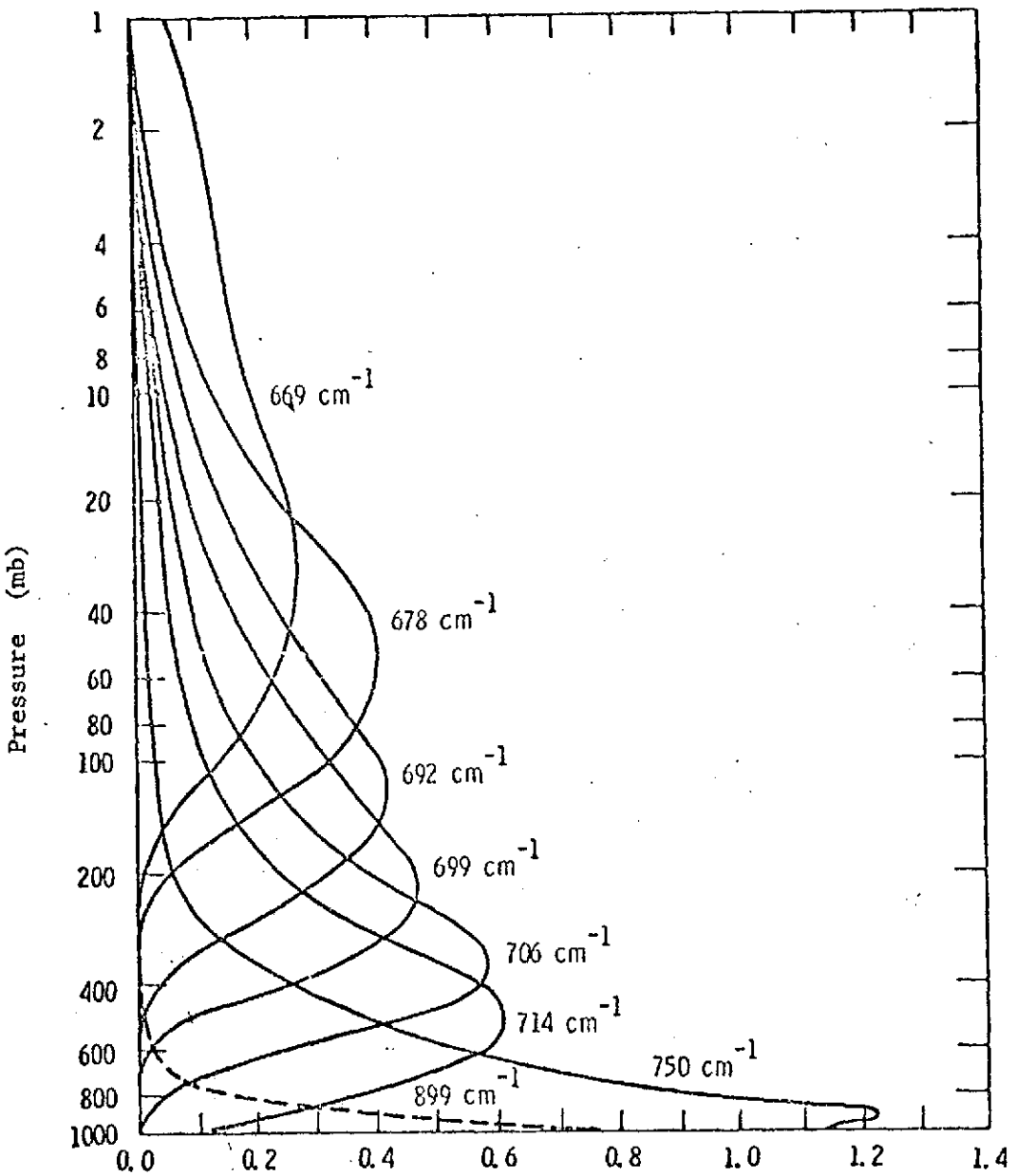
Pressure (mb)
1
2
4
6
8
10
20
40
60
80
100
200
400
600
800
1000
669 cm-1
678 cm-1
692 cm-1
699 cm-1
706 cm-1
714 cm-1
750 cm-1
899 cm-1
0.0
0.2
0.4
0.6
0.8
1.0
1.2
1.4
dT/dz

Fig. 5. The IRIS-D instrument functions, apodized and unapodized. When properly normalized, the amplitude of the apodized instrument function at $\tilde{\upsilon} = \tilde{\upsilon}_i$ is 0.54 that of the unapodized instrument function.

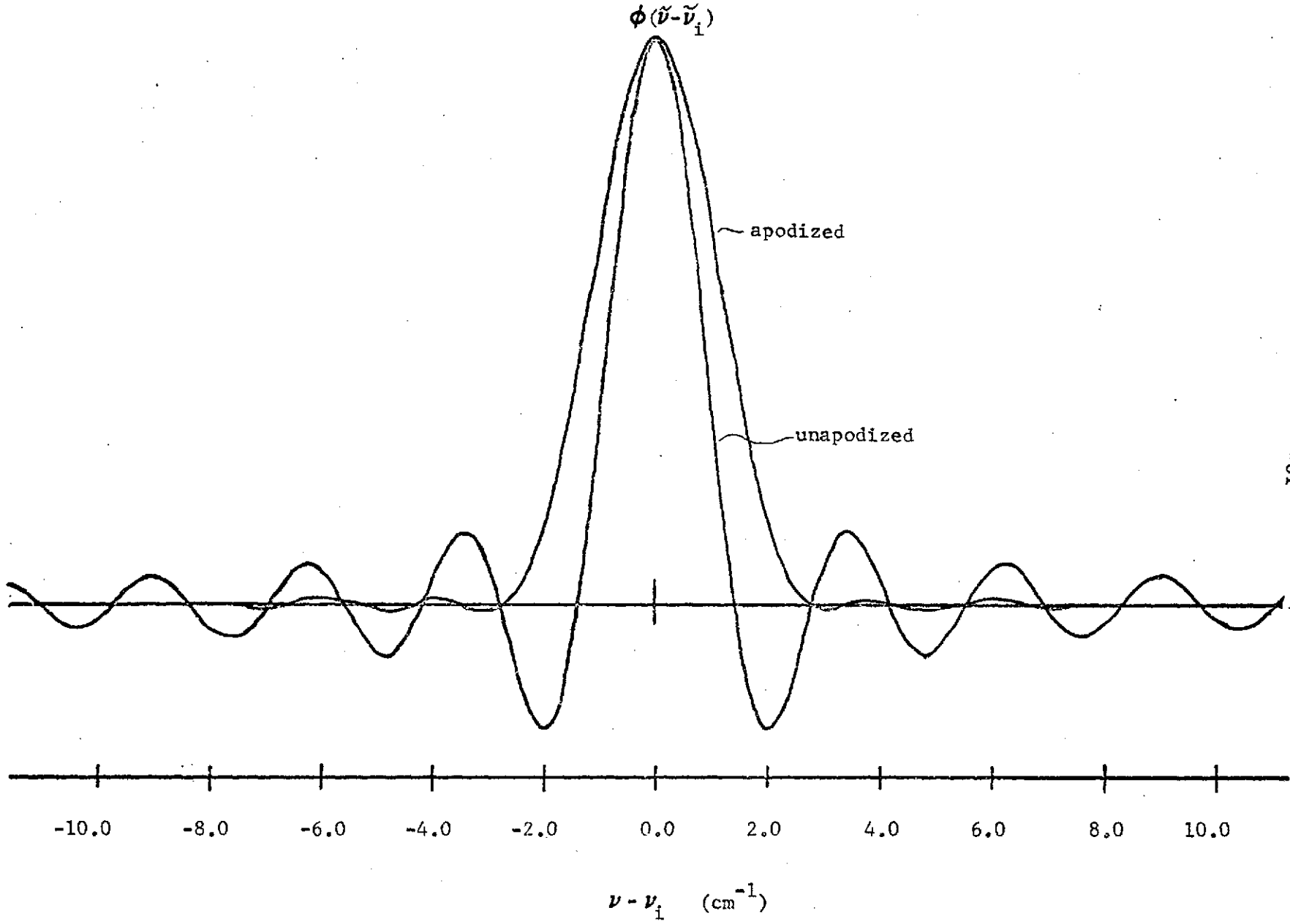
$\phi(\tilde{\nu}-\tilde{\nu}_i)$
apodized
unapodized
-10.0
-8.0
-6.0
-4.0
-2.0
0.0
2.0
4.0
6.0
8.0
10.0
$\nu - \nu_i$ (cm^{-1})

Fig. 6. The weighting functions at 668.2 cm^{-1} corresponding to the apodized and the unapodized IRIS-D instrument functions.

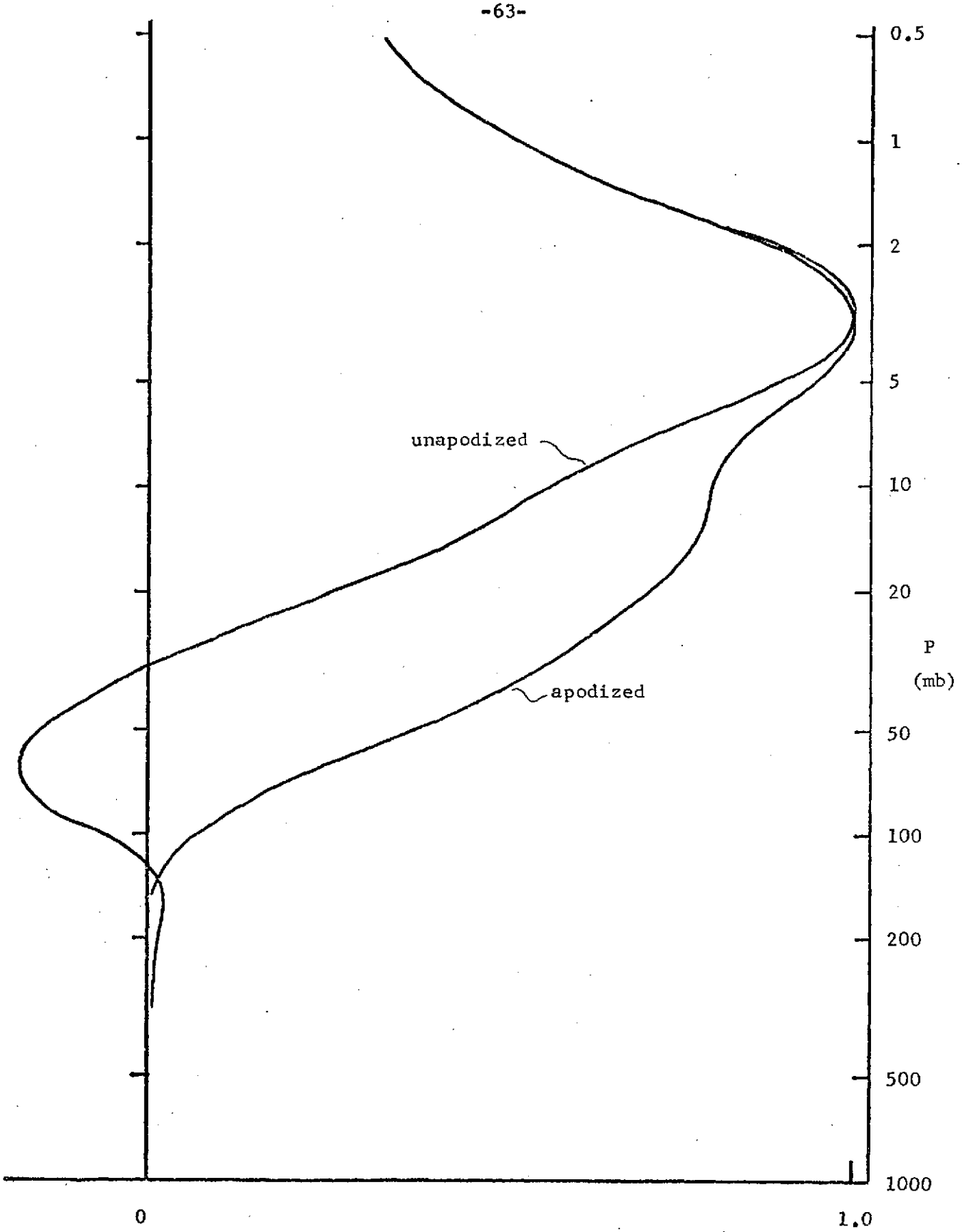
0.5
1
2
5
10
20
P
(mb)
50
100
200
500
1000
unapodized
apodized
0
1.0
$\frac{dB}{d\theta}\frac{d\bar{T}}{dz}$ (NORMALIZED)

Fig. 7. The set of ten weighting functions originally selected for this study.

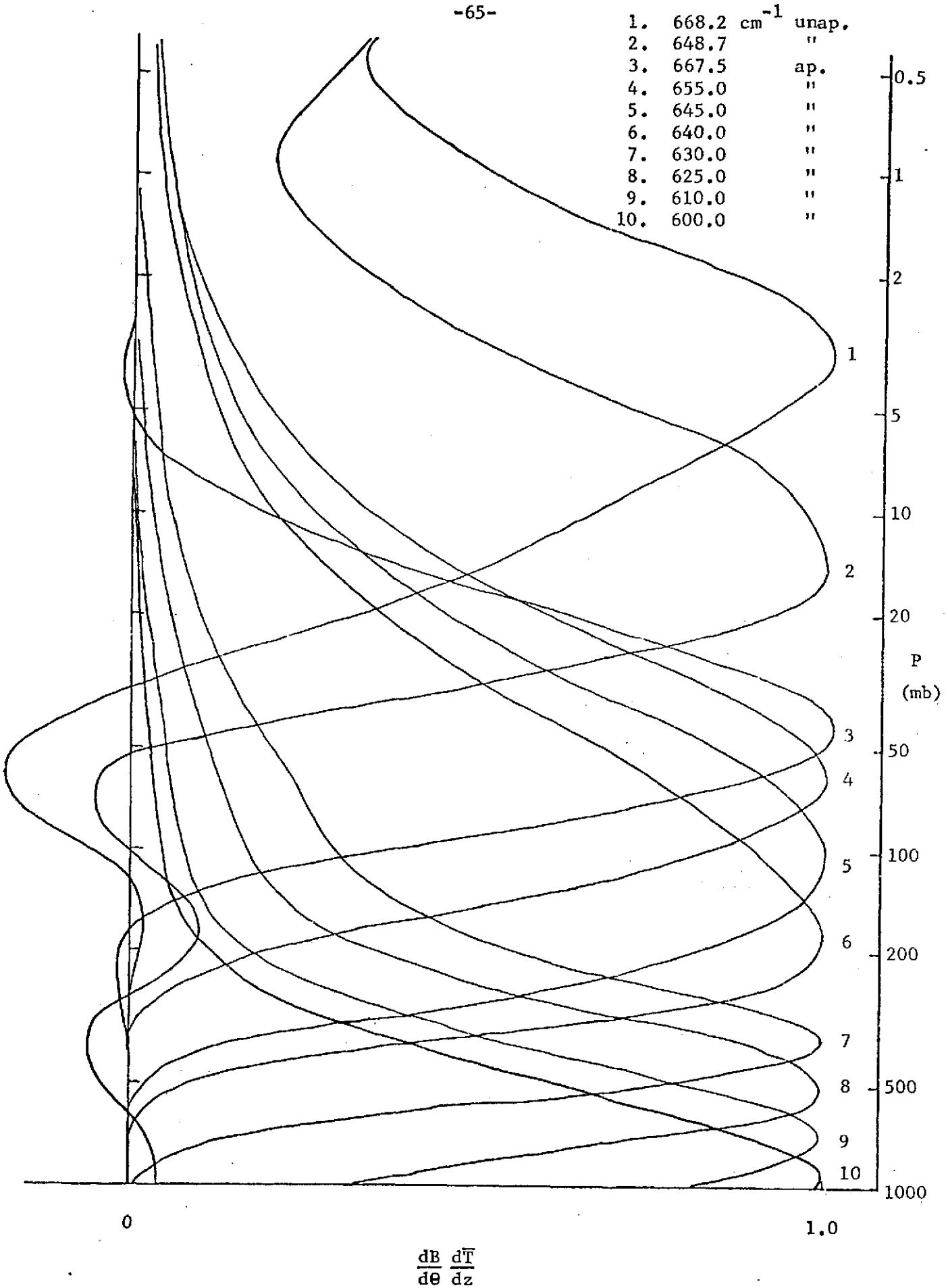
1. 668.2 cm-1 unap.
2. 648.7 "
3. 667.5 ap.
4. 655.0 "
5. 645.0 "
6. 640.0 "
7. 630.0 "
8. 625.0 "
9. 610.0 "
10. 600.0 "
0.5
1
2
5
10
20
P
(mb)
50
100
200
500
1000
1
2
3
4
5
6
7
8
9
10
0
1.0
dB/dθ dT̄/dz

Fig. 8. The temperature profile assumed in calculating the CO_2 weighting functions.

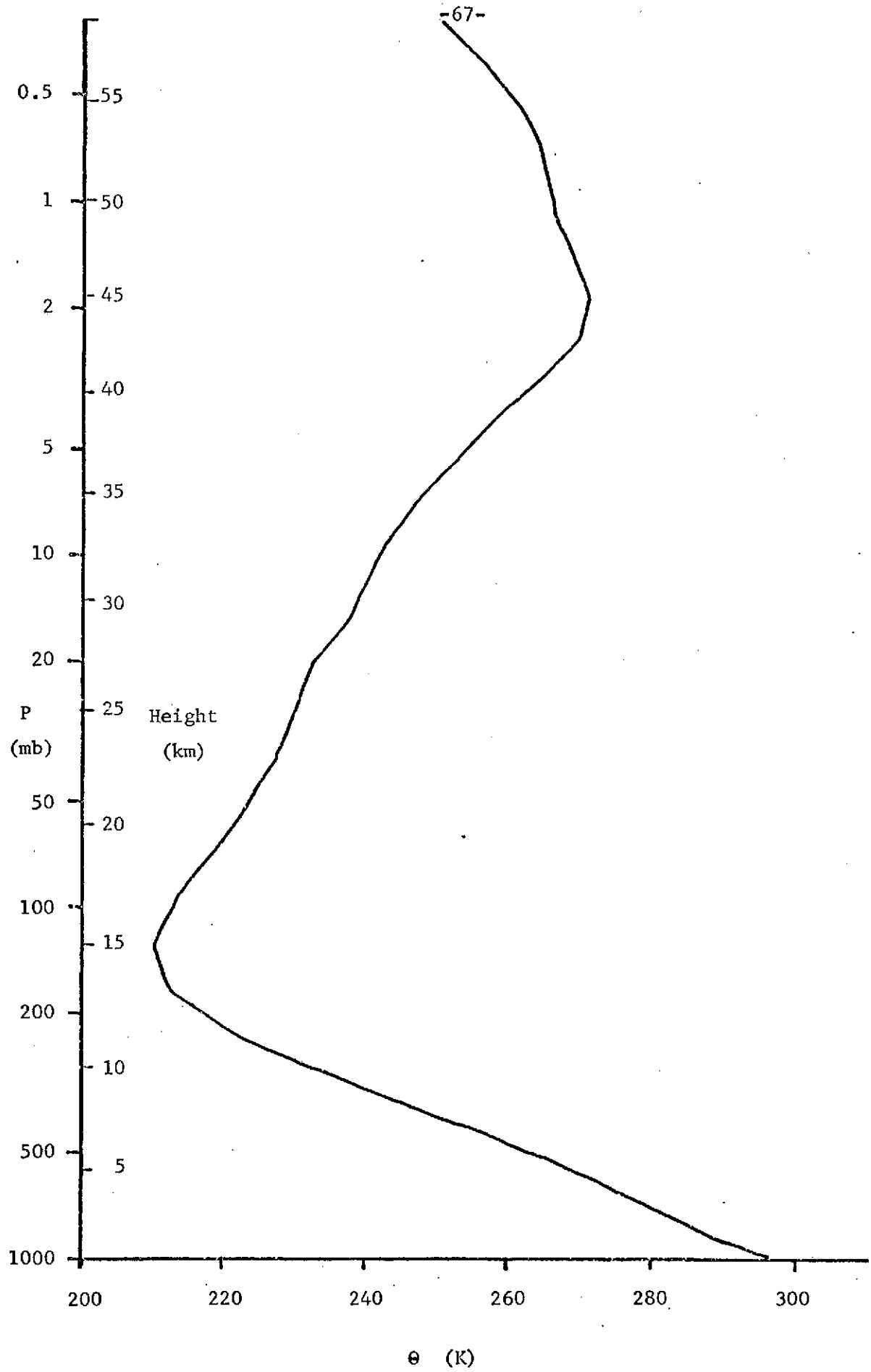
0.5
1
2
5
10
20
50
100
200
500
1000
P
(mb)
55
50
45
40
35
30
25
20
15
10
5
Height
(km)
200
220
240
260
280
300
θ (K)

Fig. 9. The weighting functions at 668.2 cm^{-1} (unapodized) and at 667.5 cm^{-1} (apodized) and their difference.

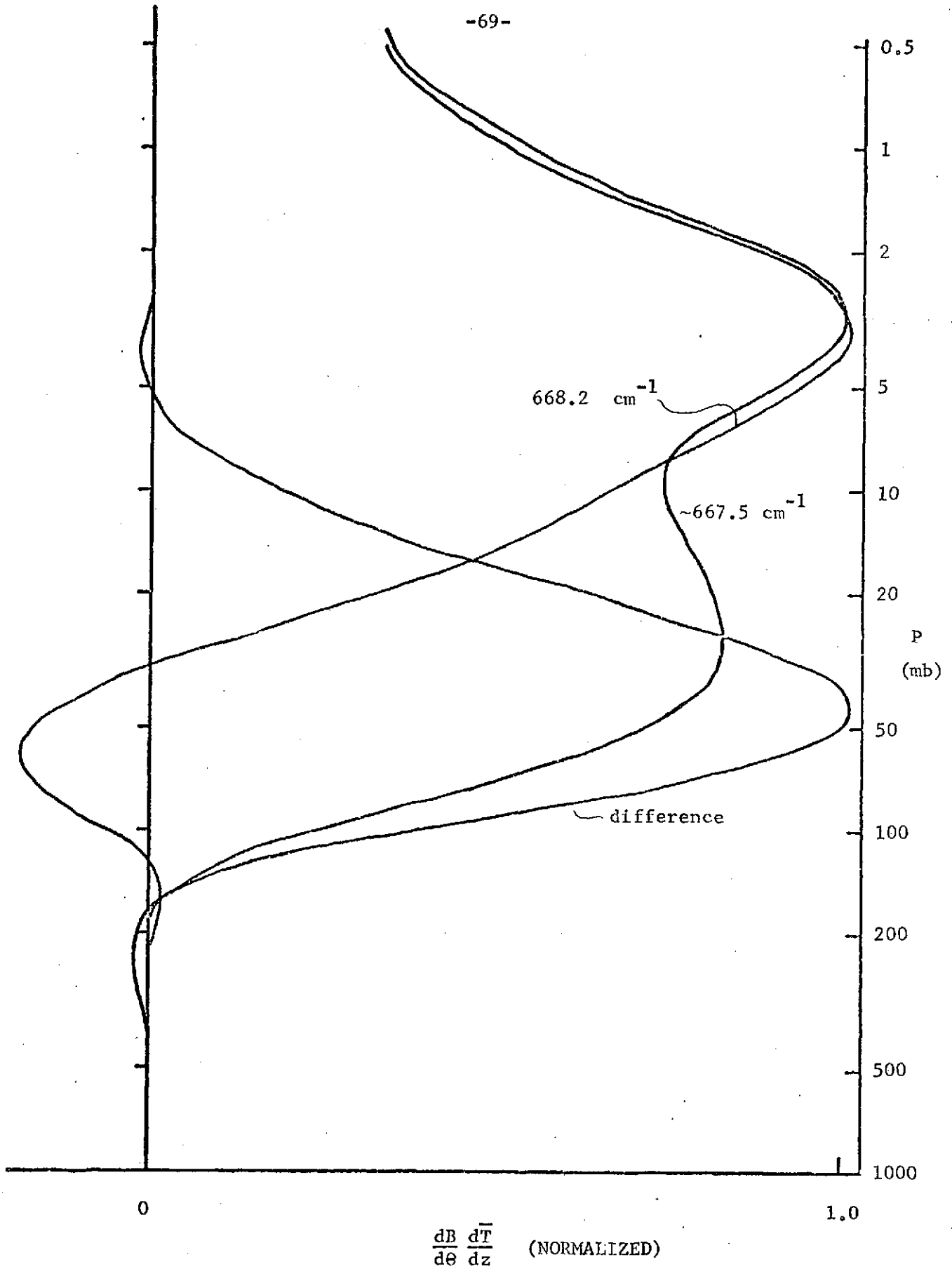
0.5
1
2
5
10
20
P
(mb)
50
100
200
500
1000
668.2 cm-1
~667.5 cm-1
difference
0
1.0
dB/dθ dT̄/dz (NORMALIZED)

Fig. 10. The final set of three weighting functions chosen for this study. An additional one at 667.4 cm^{-1}, apodized (dashed line), is also shown, but is not used in the relaxation procedure.

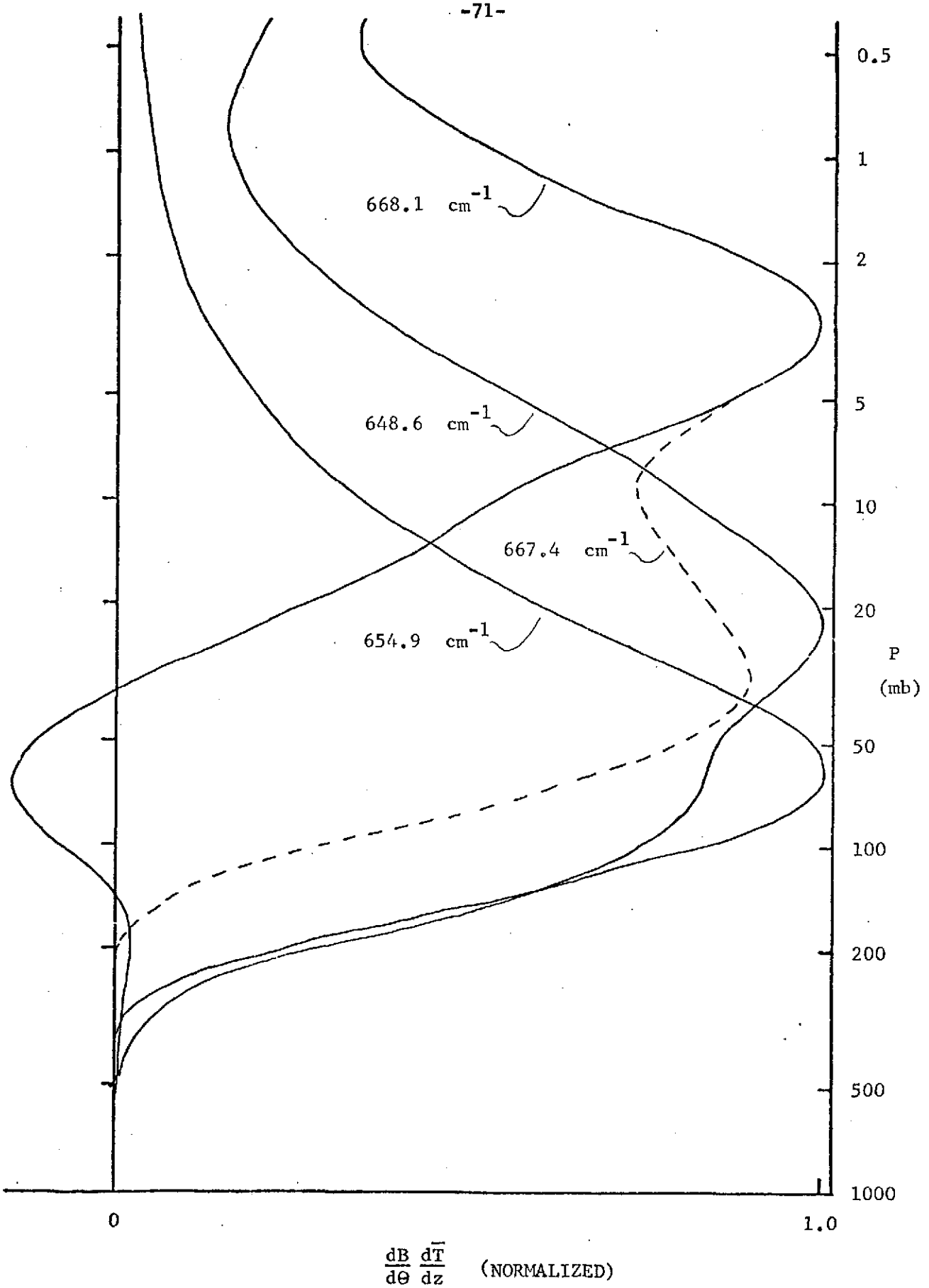
668.1 cm-1
648.6 cm-1
667.4 cm-1
654.9 cm-1
0.5
1
2
5
10
20
50
100
200
500
1000
P
(mb)
0
1.0
dB/dΘ dT̄/dz (NORMALIZED)

Fig. 11. The curves of $R^{(n)}_{rms}$ vs. n for error-free synthetic radiance data and initial guess A.

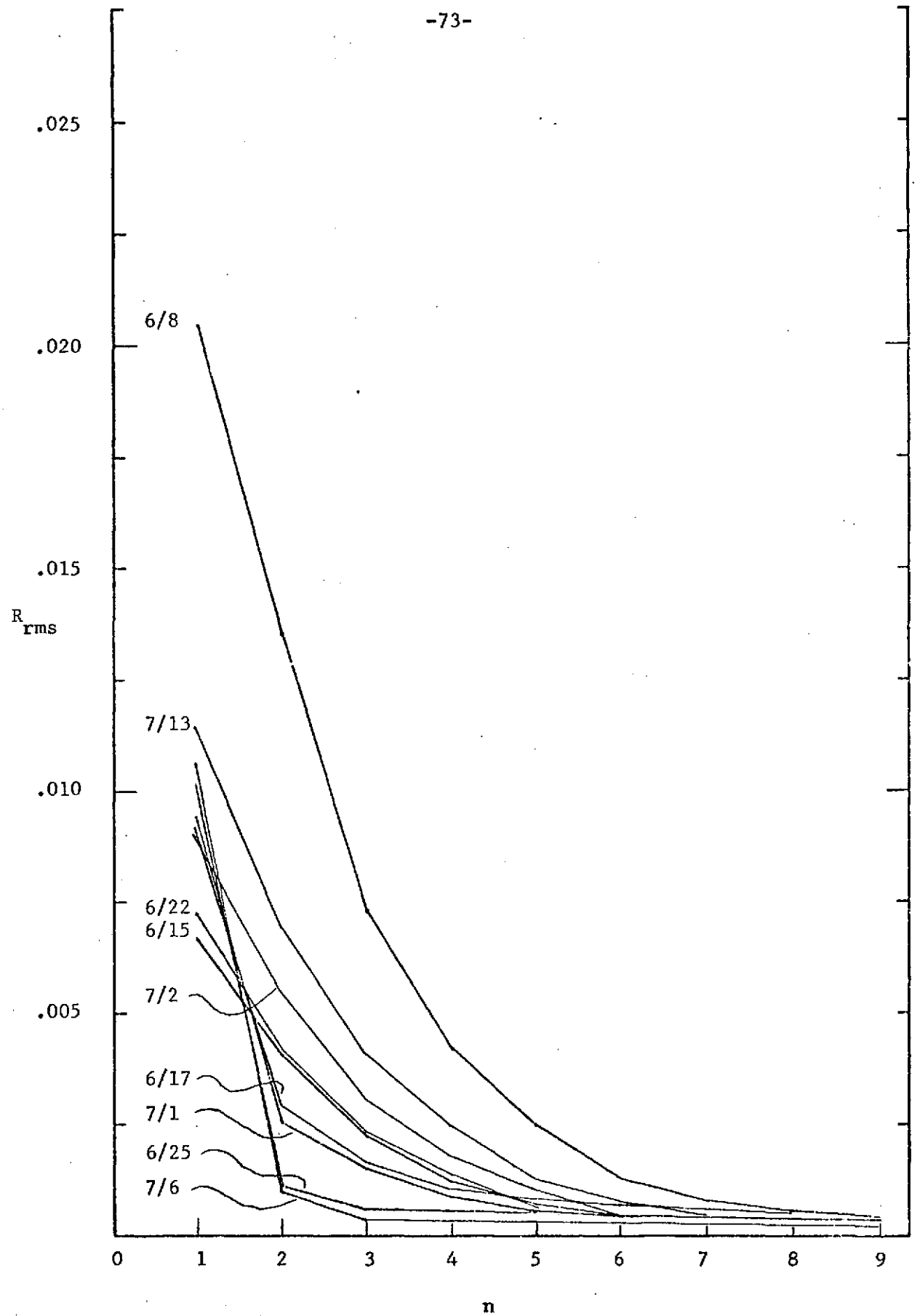
.025
.020
.015
.010
.005
R_{rms}
6/8
7/13
6/22
6/15
7/2
6/17
7/1
6/25
7/6
0
1
2
3
4
5
6
7
8
9
n

Fig. 12. The curves of $\Delta\theta^{(n)}_{rms}$ vs. n for error-free synthetic radiance data and initial guess A.

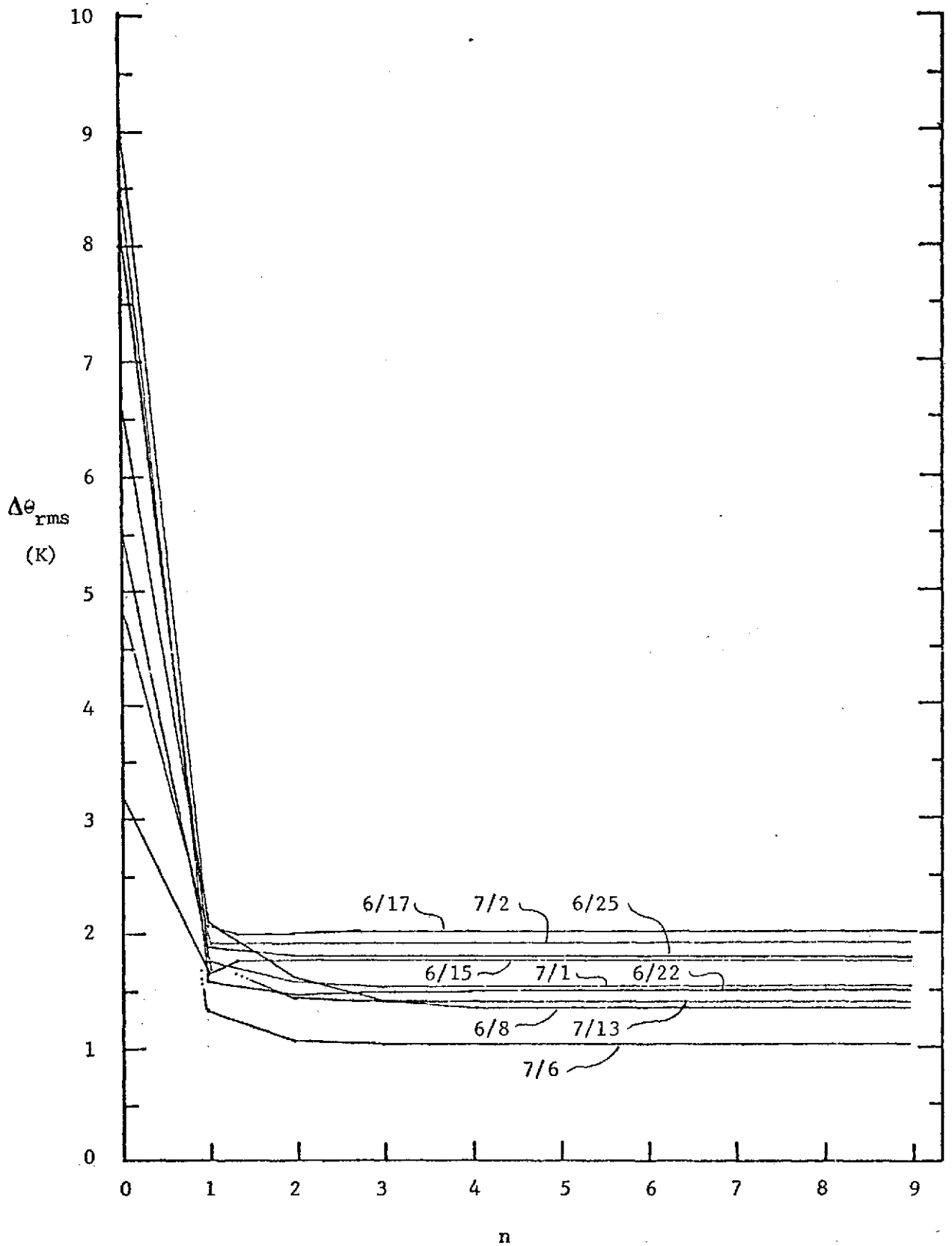
10
9
8
7
6
5
4
3
2
1
0
$\Delta\theta_{rms}$
(K)
0
1
2
3
4
5
6
7
8
9
n
6/17
7/2
6/25
6/15
7/1
6/22
6/8
7/13
7/6

Fig. 13. The curves of $R^{(n)}_{rms}$ vs. n for error-free synthetic radiance data and initial guess B.

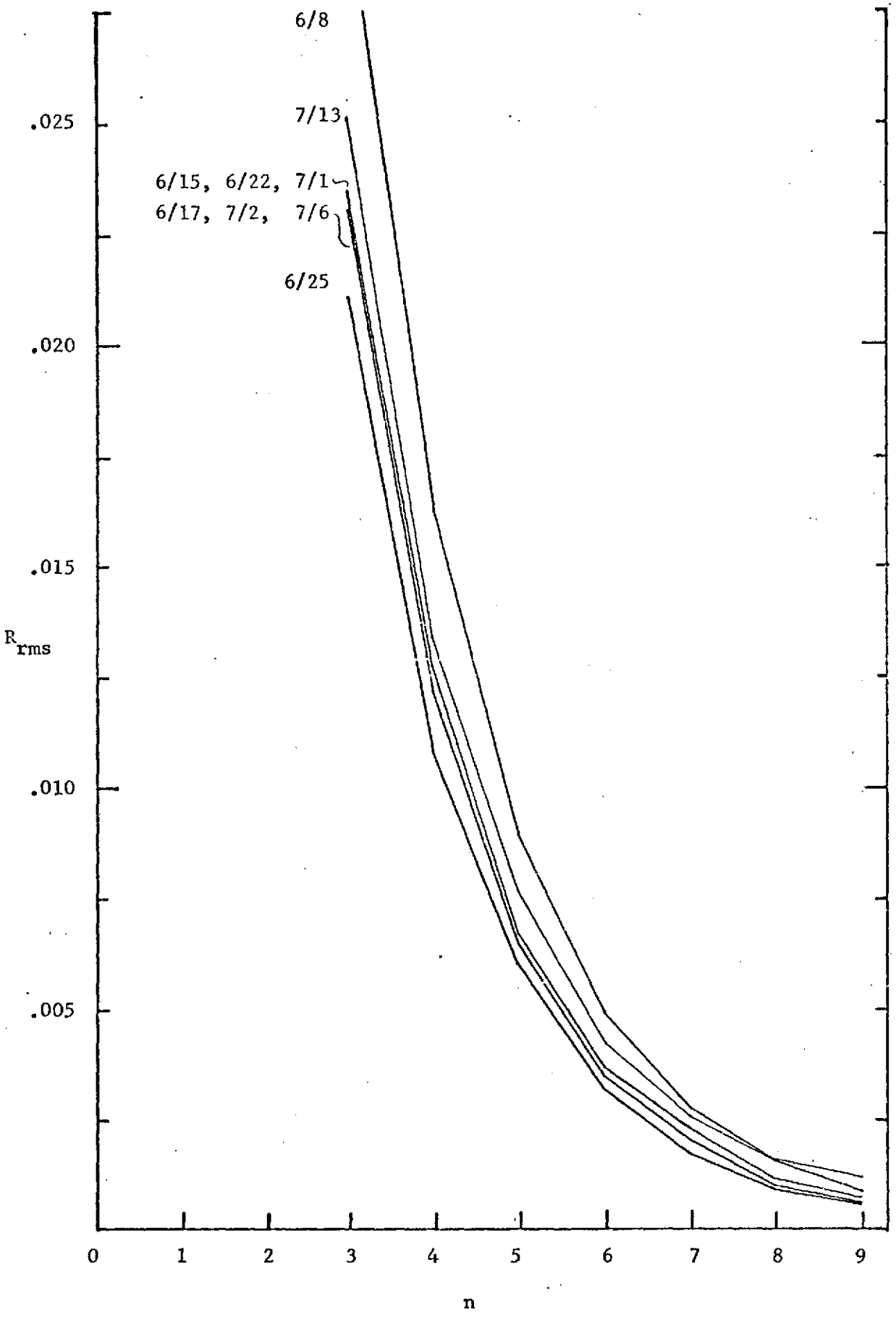
6/8
7/13
6/15, 6/22, 7/1
6/17, 7/2, 7/6
6/25
.025
.020
.015
.010
.005
R_{rms}
0
1
2
3
4
5
6
7
8
9
n

Fig. 14. The curves of $\Delta\theta^{(n)}_{rms}$ vs. n for error-free synthetic radiance data and initial guess B.

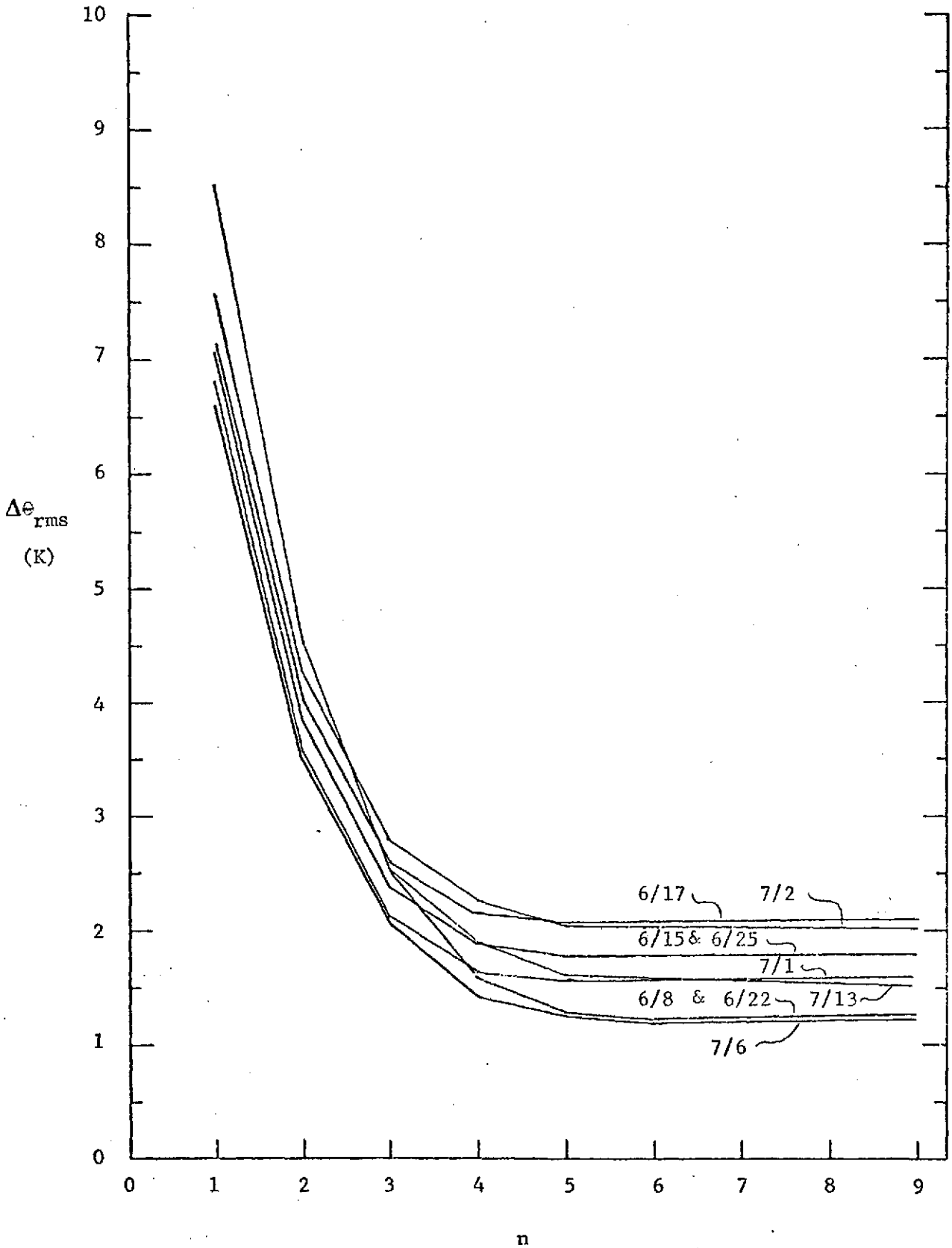
10
9
8
7
6
5
4
3
2
1
0
$\Delta\theta_{rms}$
(K)
0
1
2
3
4
5
6
7
8
9
n
6/17
7/2
6/15 & 6/25
7/1
6/8 & 6/22
7/13
7/6

Fig. 15. The *in situ* profile and the retrieved profile for error-free synthetic radiance data for 6/25, and initial guess A.

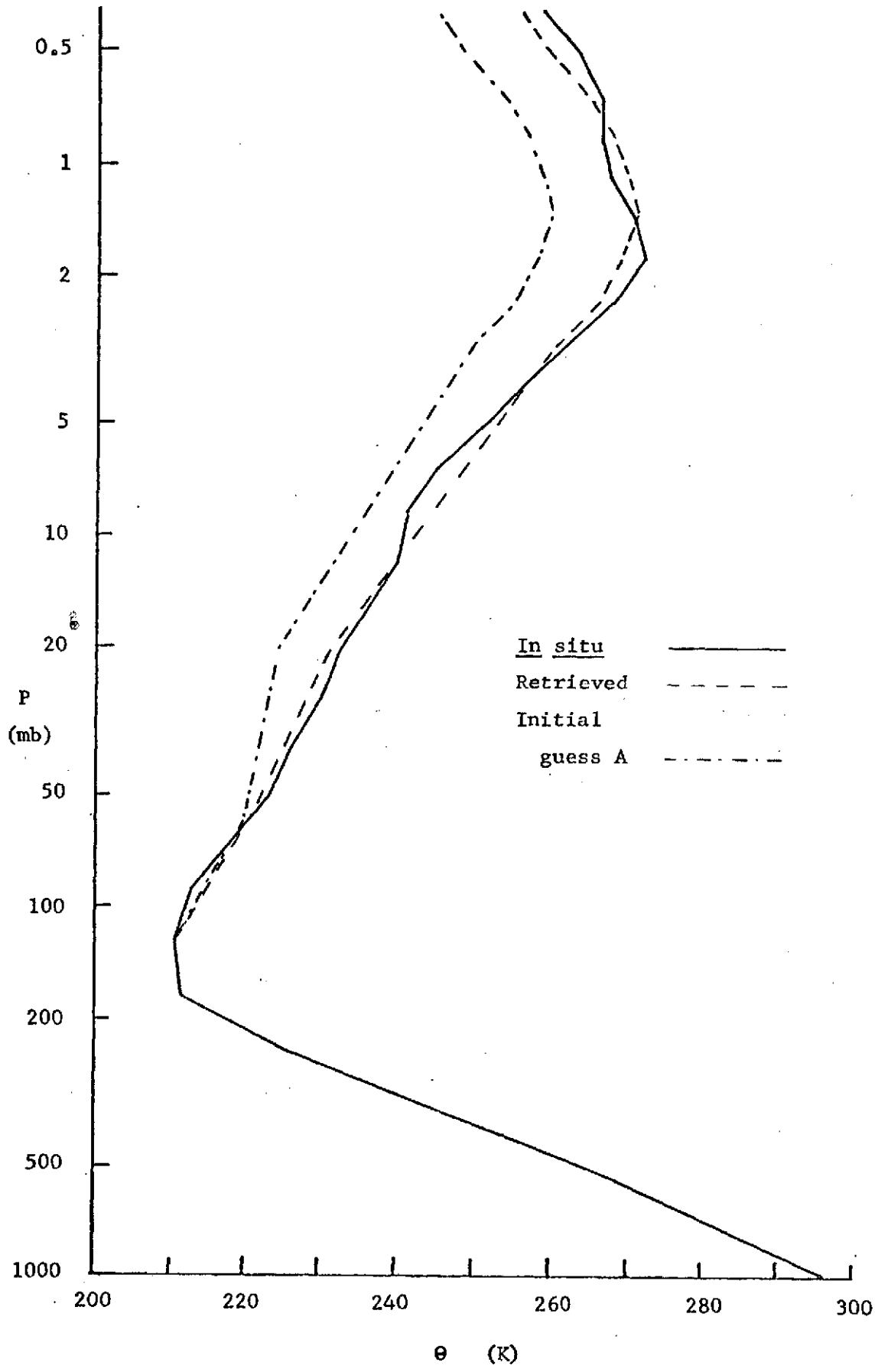
0.5
1
2
5
10
20
50
100
200
500
1000
P
(mb)
200
220
240
260
280
300
θ (K)
In situ
Retrieved
Initial
guess A

Fig. 16. The curves of $R^{(n)}_{rms}$ for the synthetic radiance data for 6/25 with six sets of 1 percent random noise and using initial guess A.

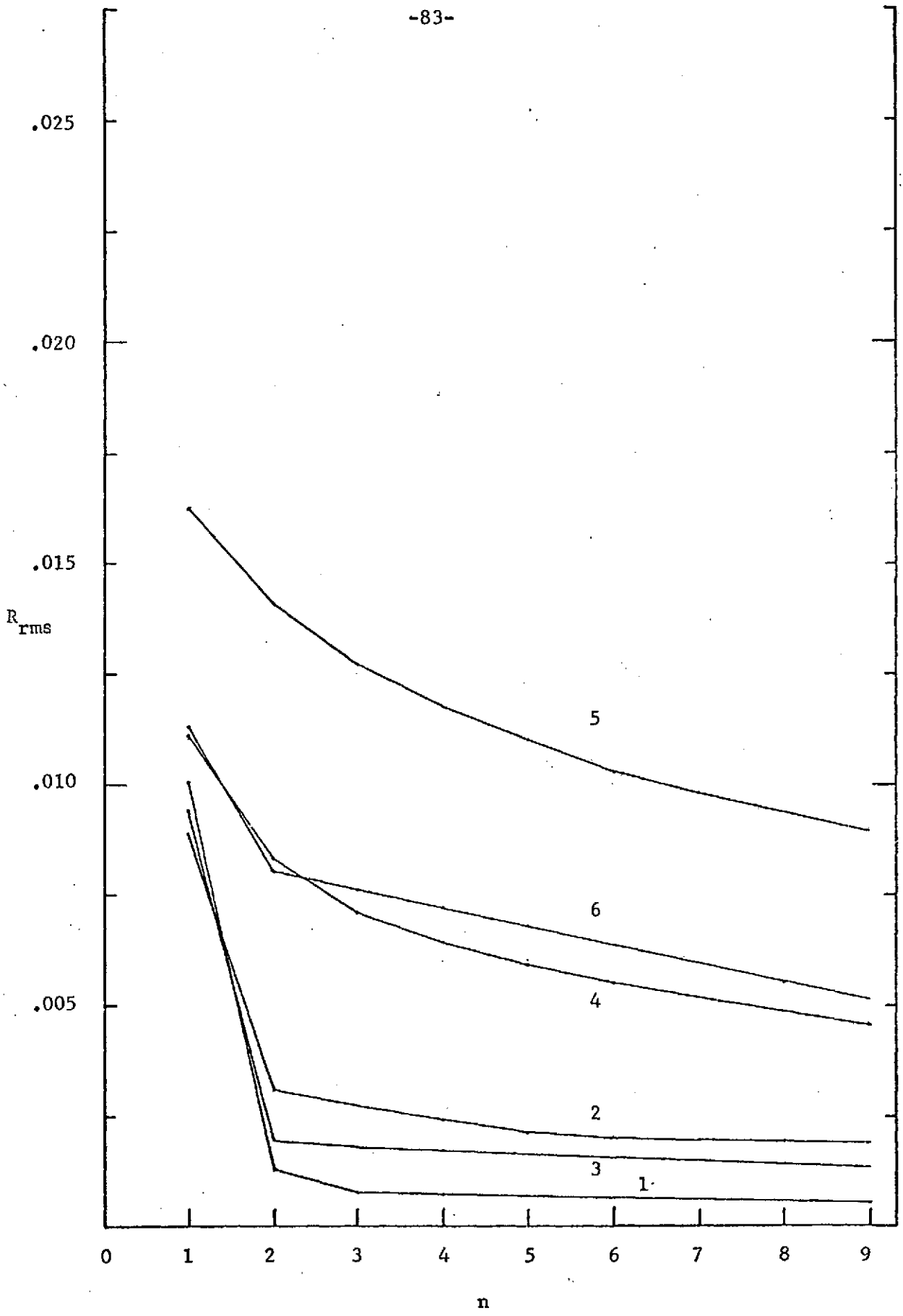
.025
.020
.015
.010
.005
R_{rms}
5
6
4
2
3
1
0
1
2
3
4
5
6
7
8
9
n

Fig. 17. The curves of $\Delta\theta^{(n)}_{rms}$ for the synthetic radiance data for 6/25 with six sets of 1 percent random noise and using initial guess A.

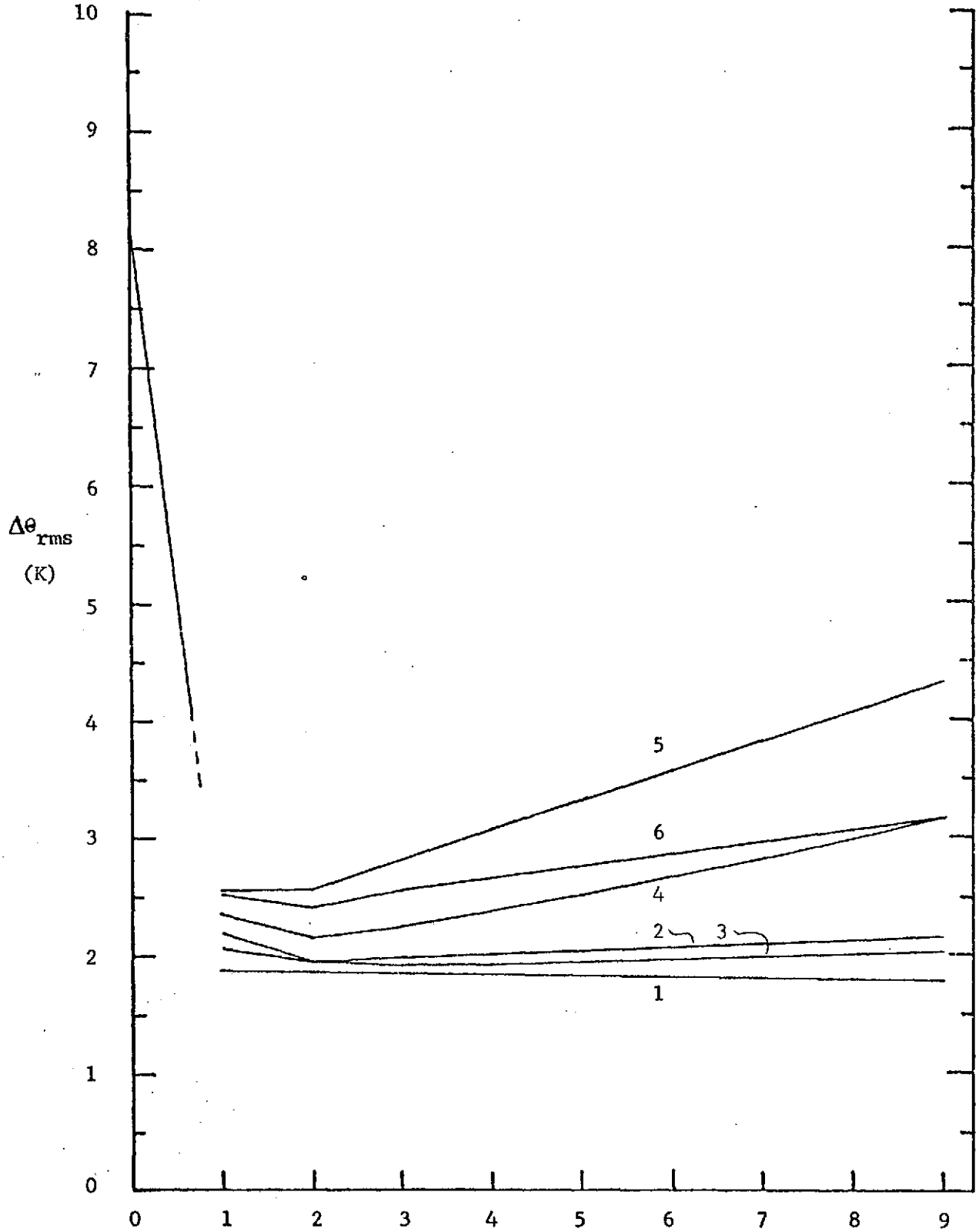
10
9
8
7
6
5
4
3
2
1
0
$\Delta\theta_{rms}$
(K)
0
1
2
3
4
5
6
7
8
9
5
6
4
2
3
1

Fig. 18. The curves of $R^{(n)}_{rms}$ for the synthetic radiance data for 6/25 with six sets of 1 percent random noise and using initial guess B.

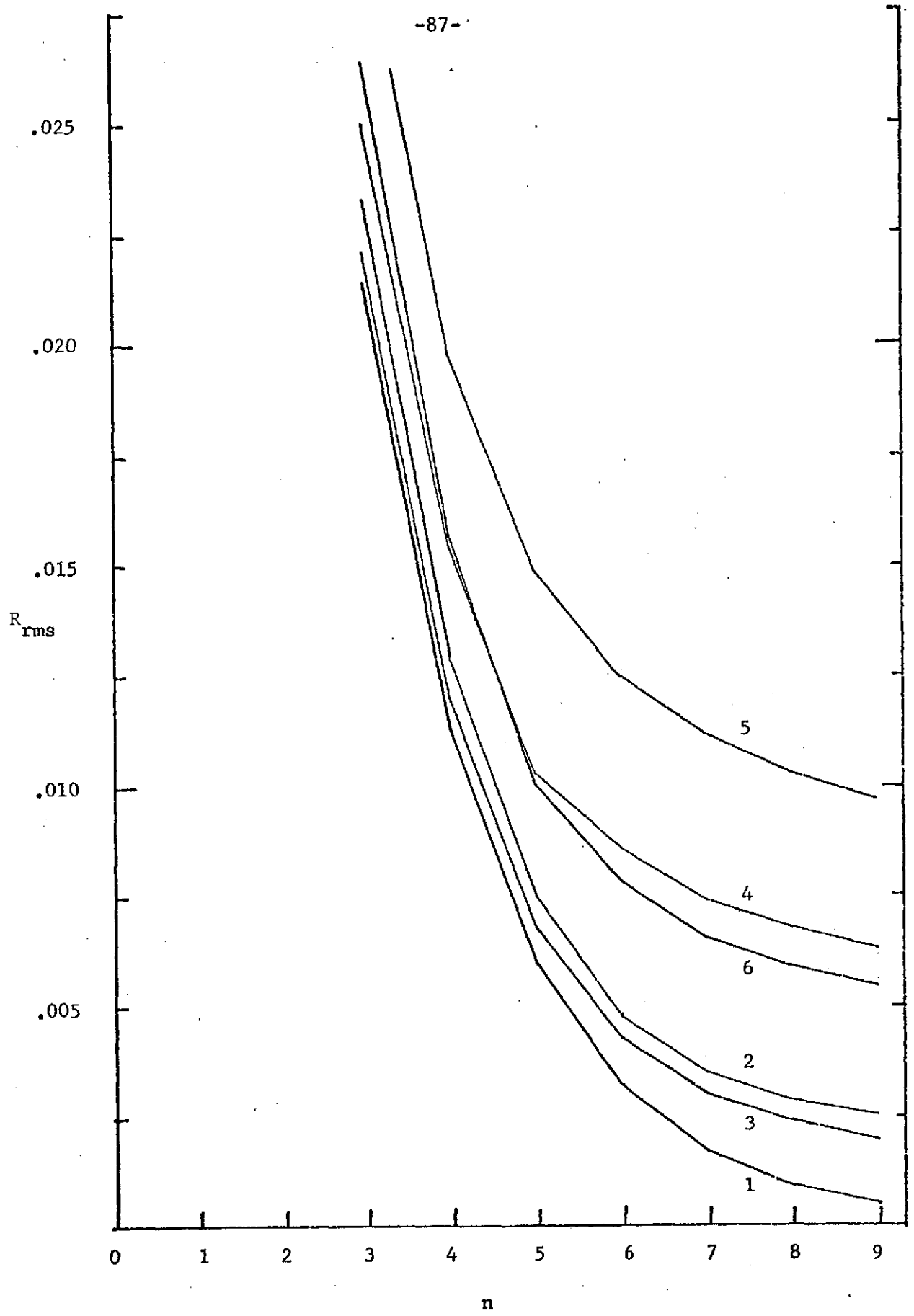
.025
.020
.015
.010
.005
R_{rms}
0
1
2
3
4
5
6
7
8
9
n
5
4
6
2
3
1

Fig. 19. The curves of $\Delta\theta^{(n)}_{rms}$ for the synthetic radiance data for 6/25 with six sets of 1 percent random noise and using initial guess B.

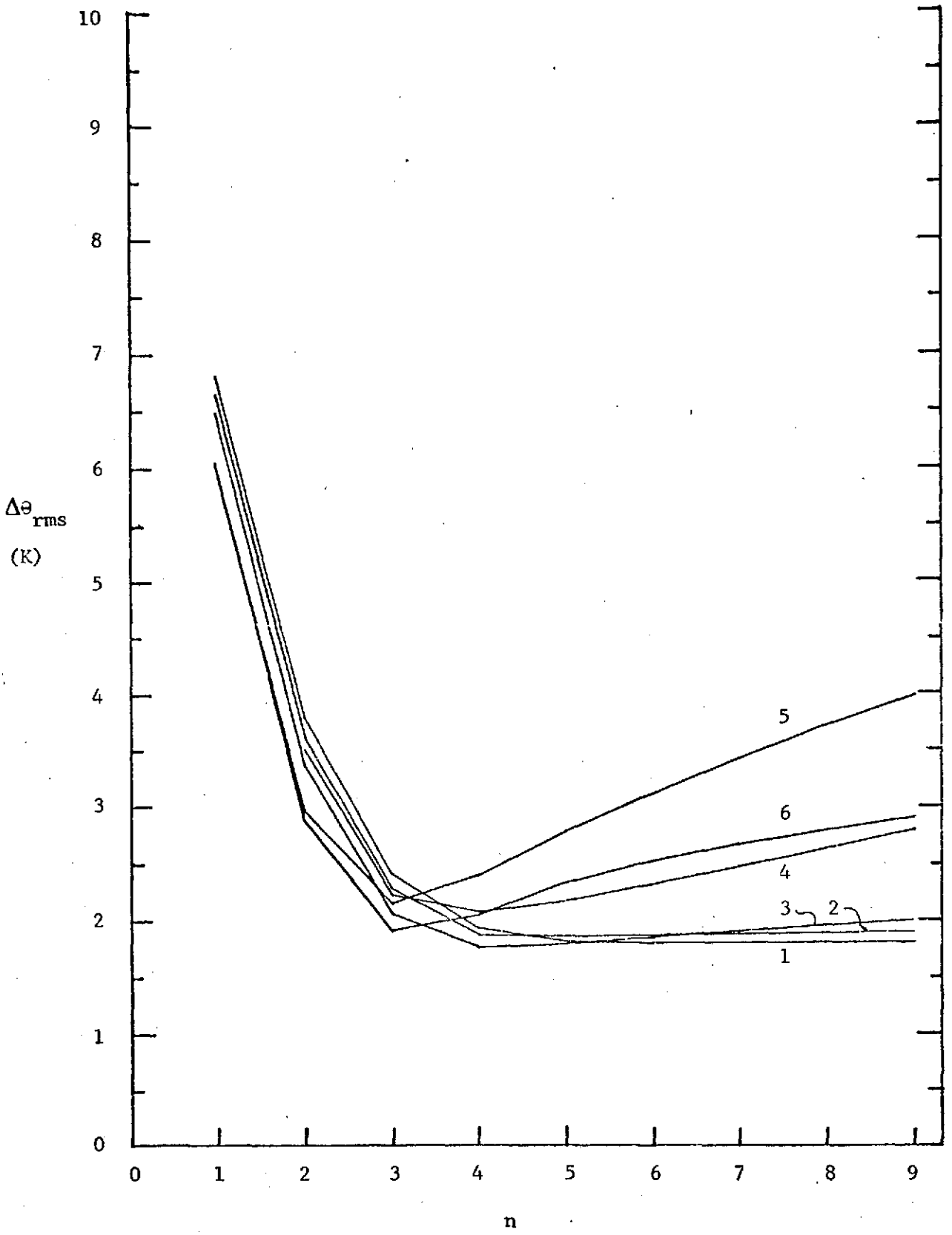
10
9
8
7
6
5
4
3
2
1
0
$\Delta\theta_{rms}$
(K)
0
1
2
3
4
5
6
7
8
9
n
5
6
4
3
2
1

Fig. 20. The curves of $R^{(n)}_{rms}$ vs. n for the actual IRIS data using initial guess A.

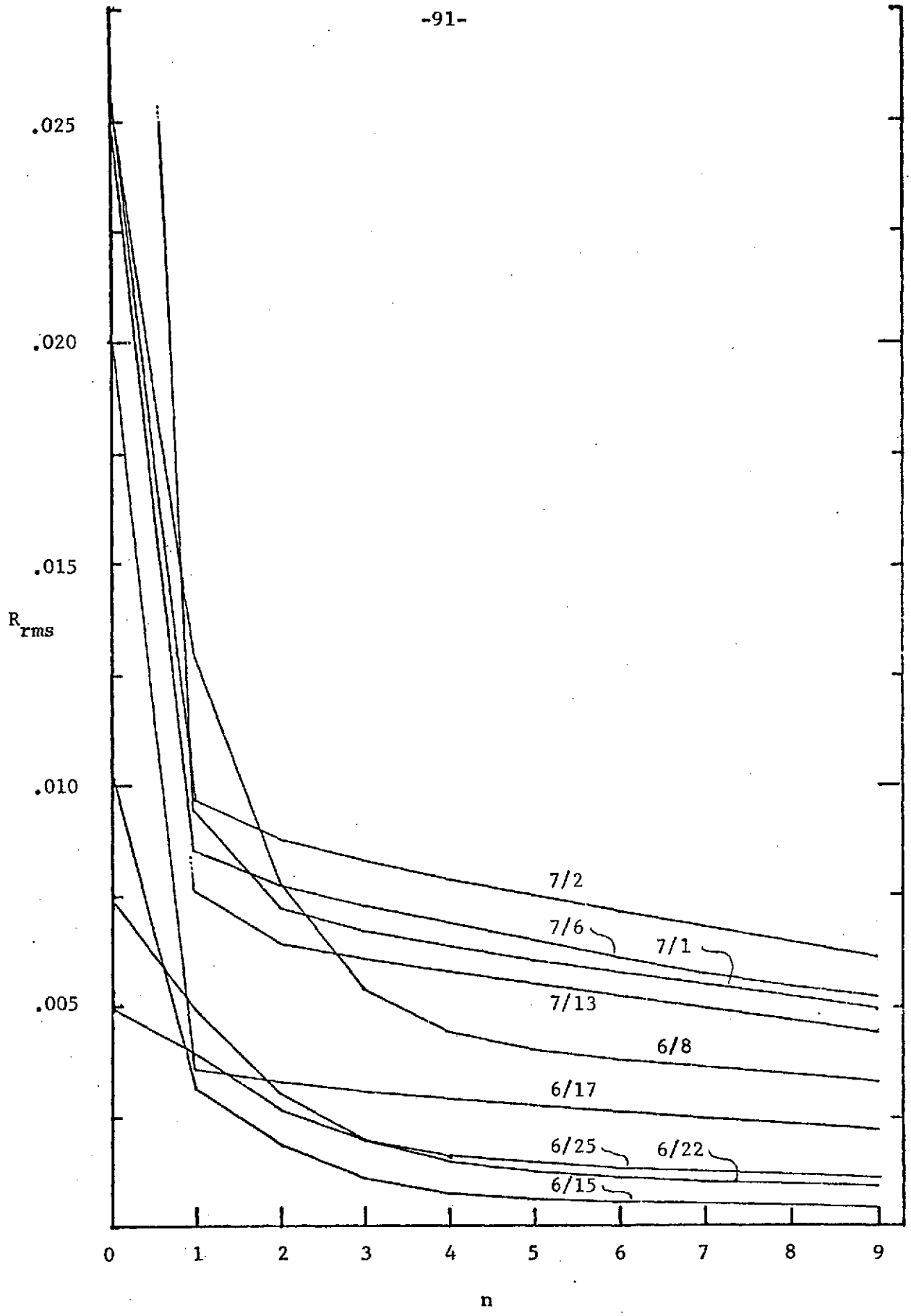
.025
.020
.015
.010
.005
R_{rms}
7/2
7/6
7/1
7/13
6/8
6/17
6/25
6/22
6/15
0
1
2
3
4
5
6
7
8
9
n

Fig. 21 (a. through i). The retrieved and the *in situ* profiles for the nine cases using the actual IRIS data and initial guess A.

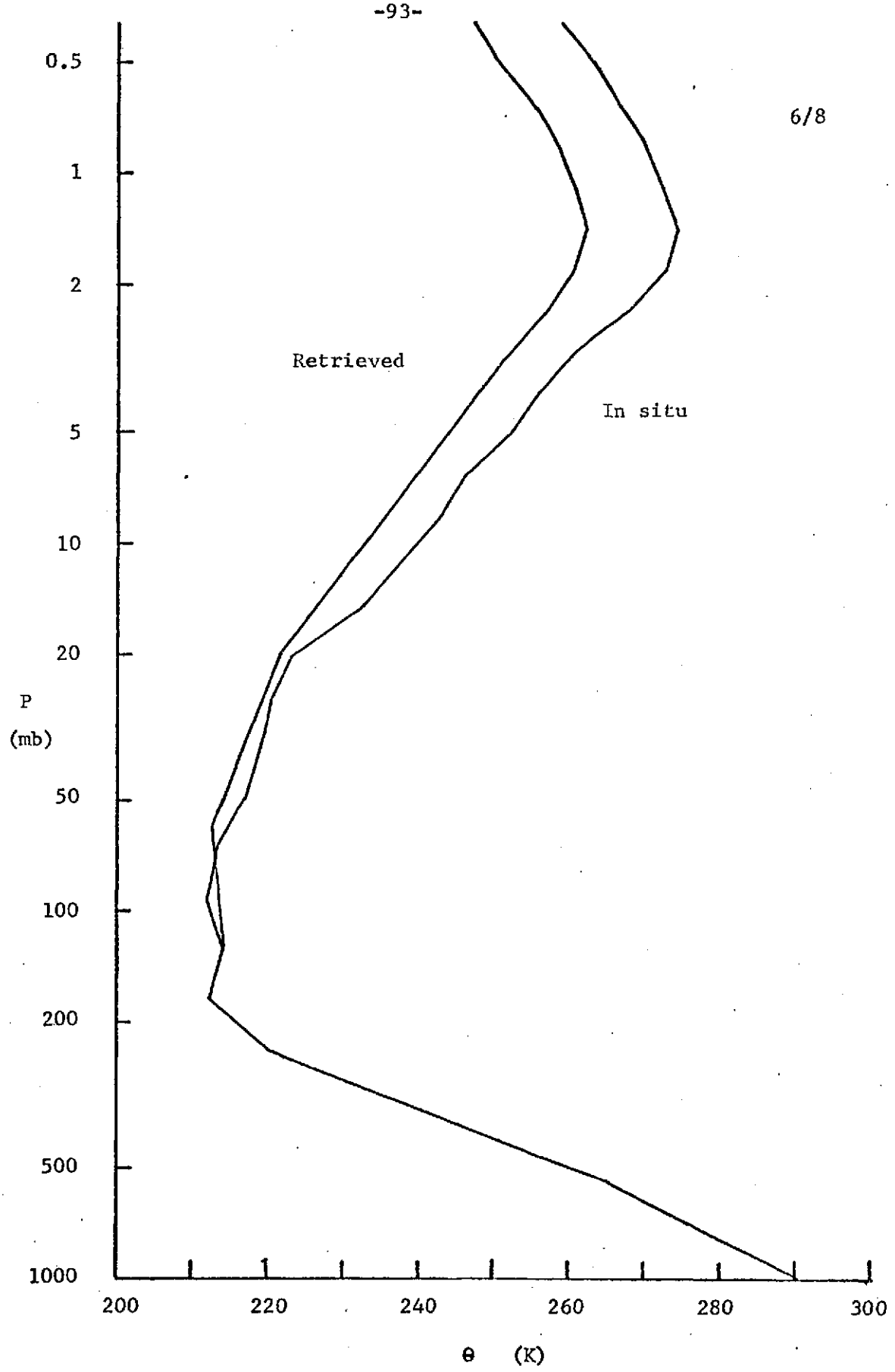
6/8
Retrieved
In situ
0.5
1
2
5
10
20
50
100
200
500
1000
P
(mb)
200
220
240
260
280
300
θ (K)

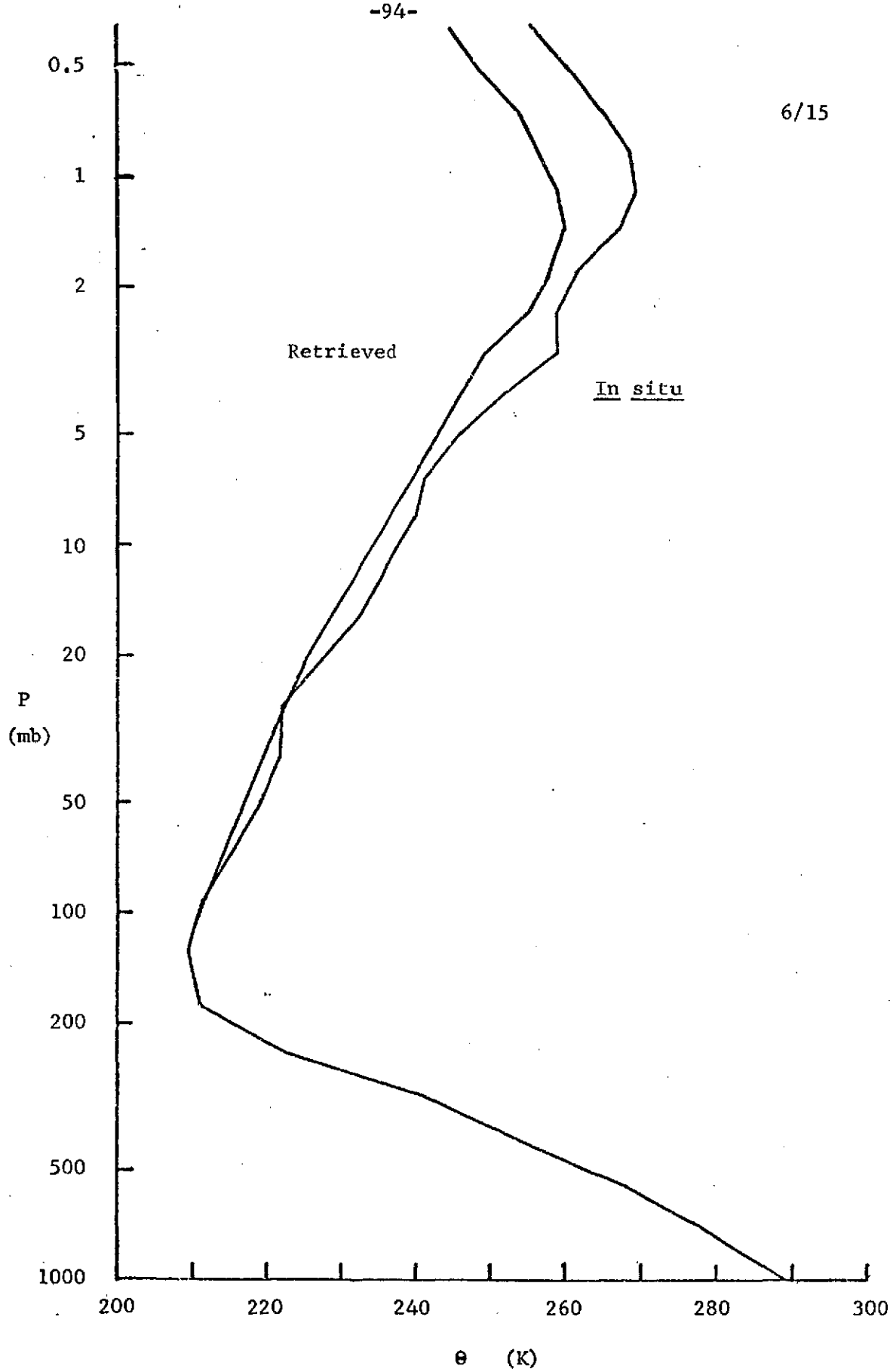
6/15
0.5
1
2
5
10
20
50
100
200
500
1000
P
(mb)
Retrieved
In situ
200
220
240
260
280
300
θ (K)

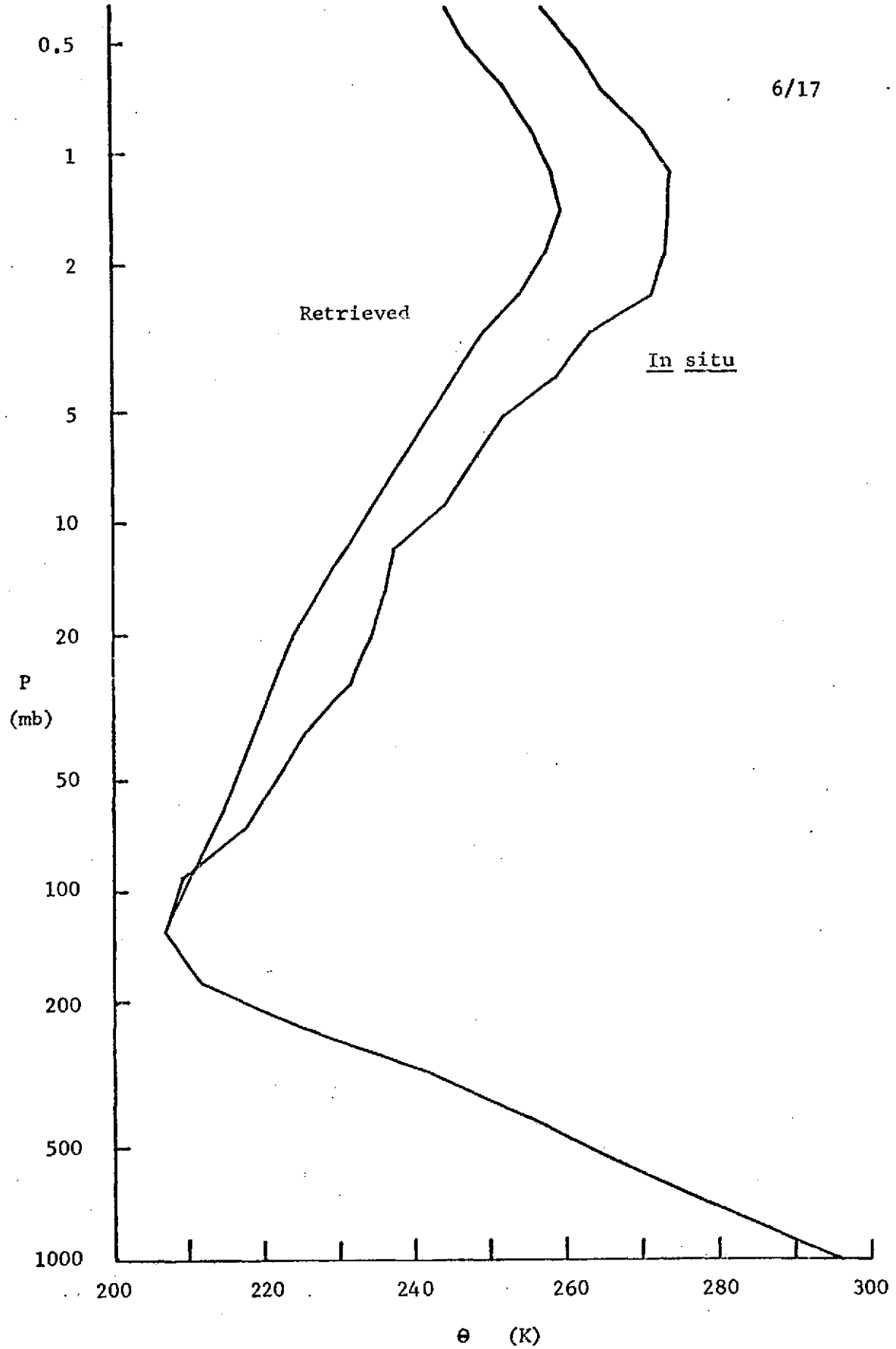
6/17
Retrieved
In situ
0.5
1
2
5
10
20
P
(mb)
50
100
200
500
1000
200
220
240
260
280
300
θ (K)

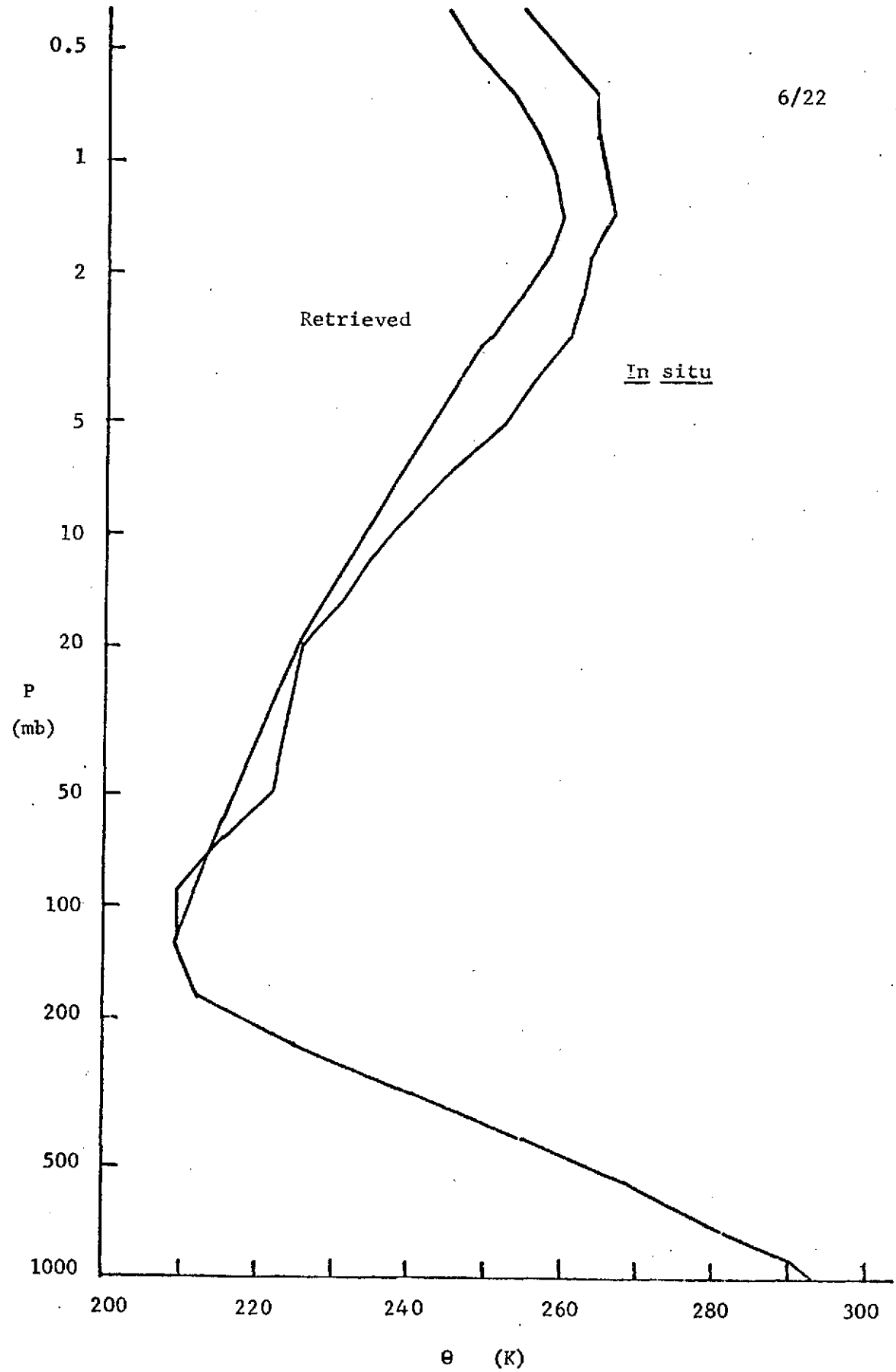
6/22
Retrieved
In situ
0.5
1
2
5
10
20
50
100
200
500
1000
P
(mb)
200
220
240
260
280
300
θ (K)

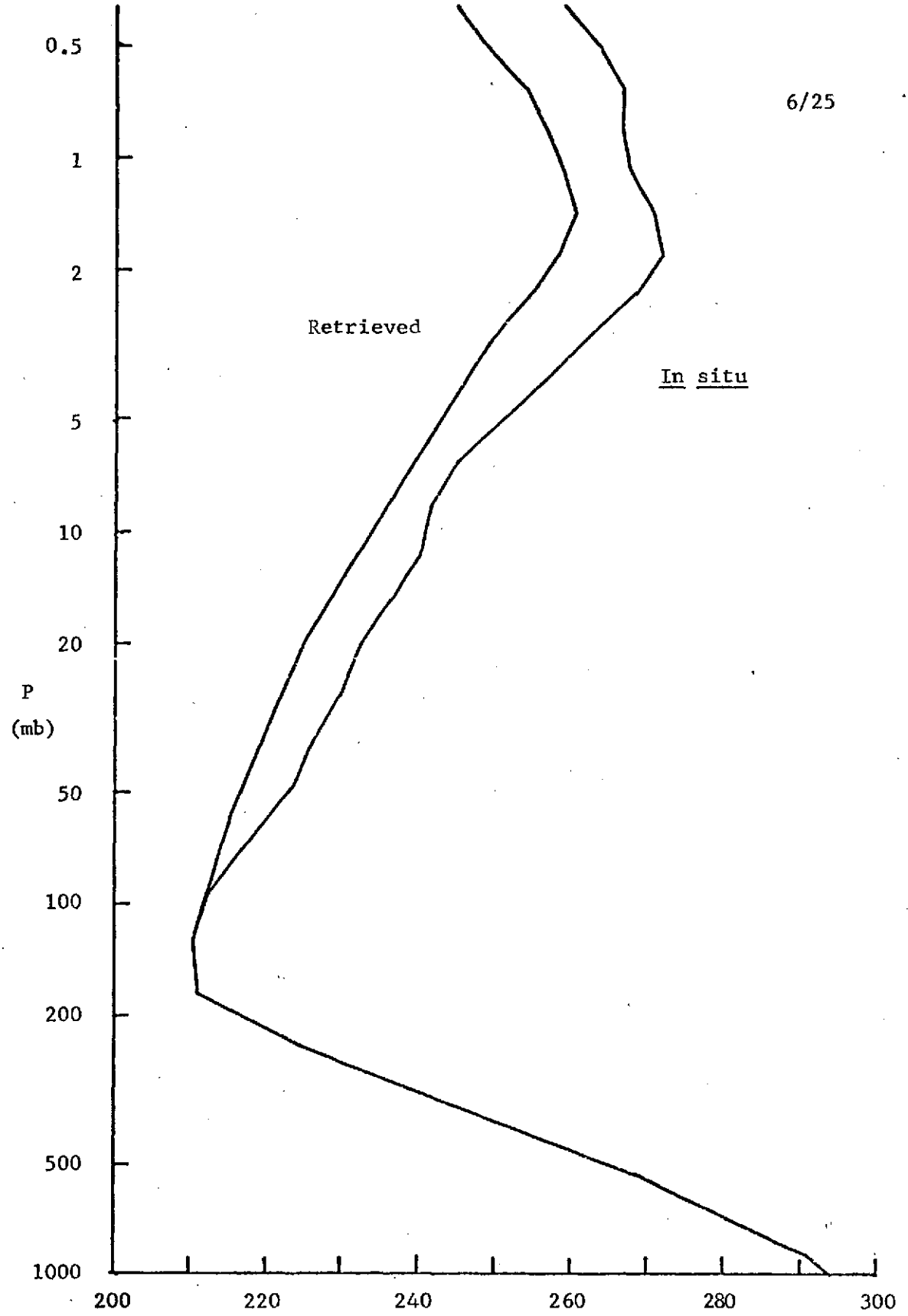
6/25
Retrieved
In situ
P
(mb)
0.5
1
2
5
10
20
50
100
200
500
1000
200
220
240
260
280
300

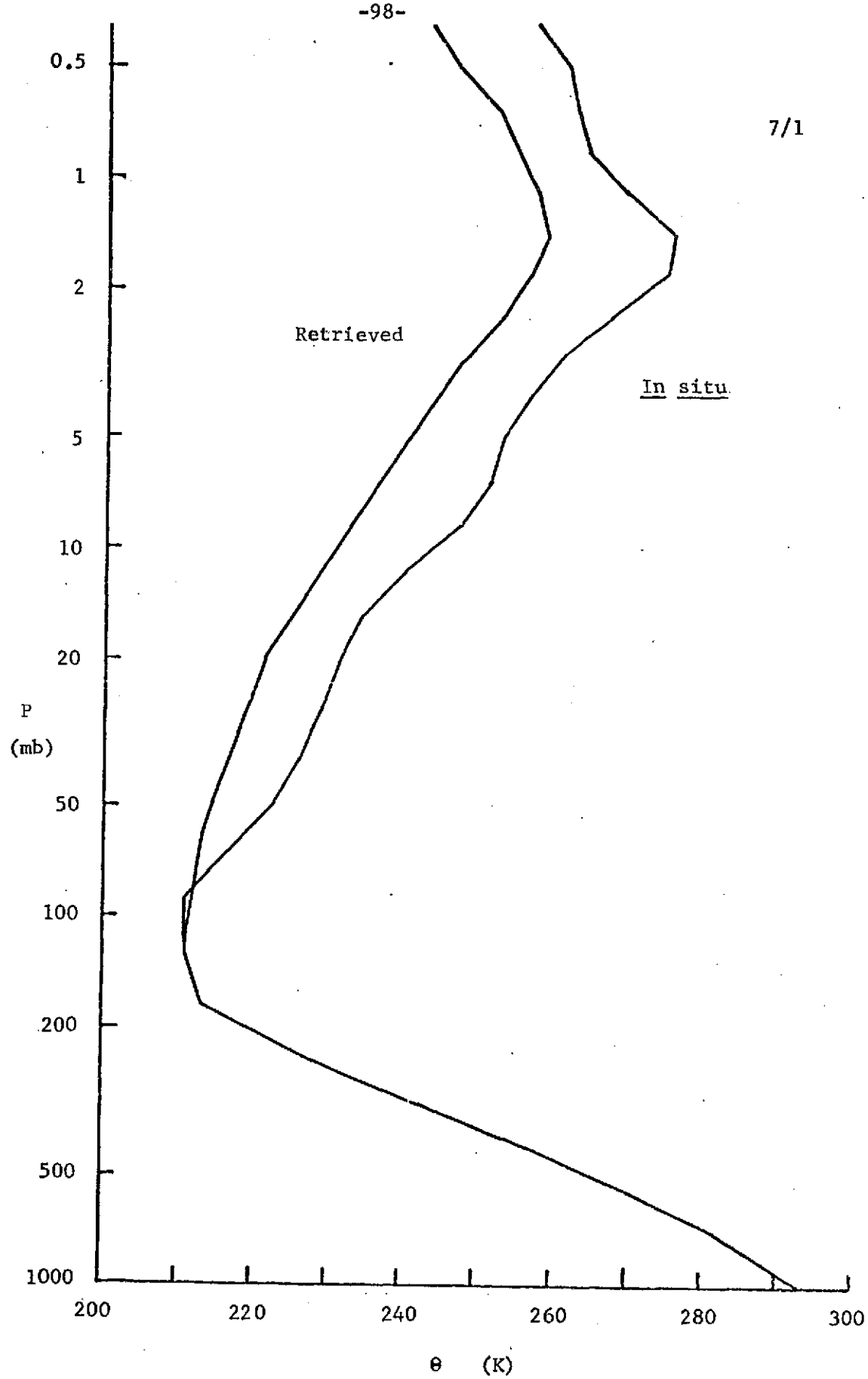
7/1
Retrieved
In situ
0.5
1
2
5
10
20
P
(mb)
50
100
200
500
1000
200
220
240
260
280
300
θ (K)

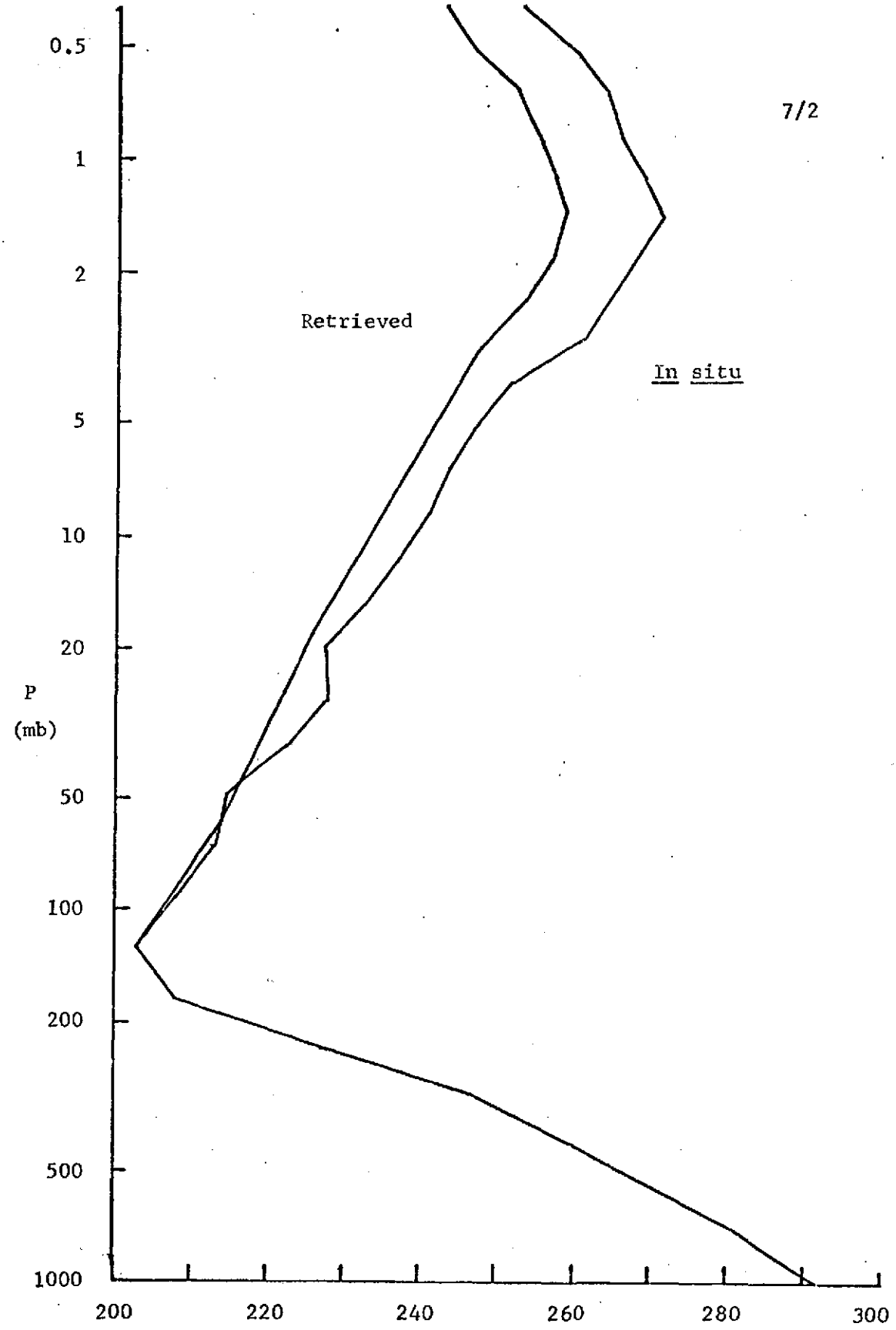
7/2
Retrieved
In situ
P
(mb)
0.5
1
2
5
10
20
50
100
200
500
1000
200
220
240
260
280
300

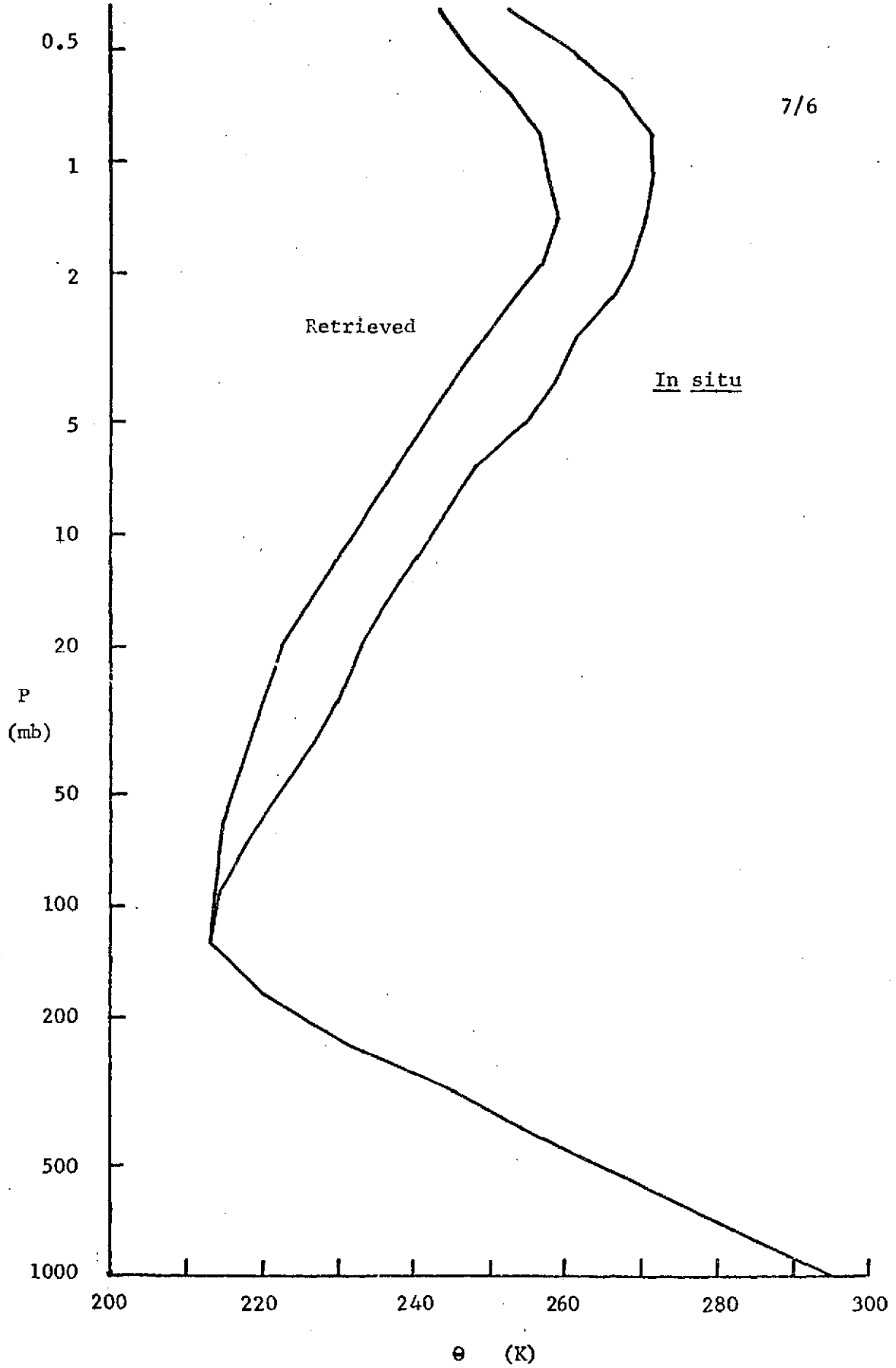
7/6
Retrieved
In situ
0.5
1
2
5
10
20
P
(mb)
50
100
200
500
1000
200
220
240
260
280
300
θ (K)

7/13

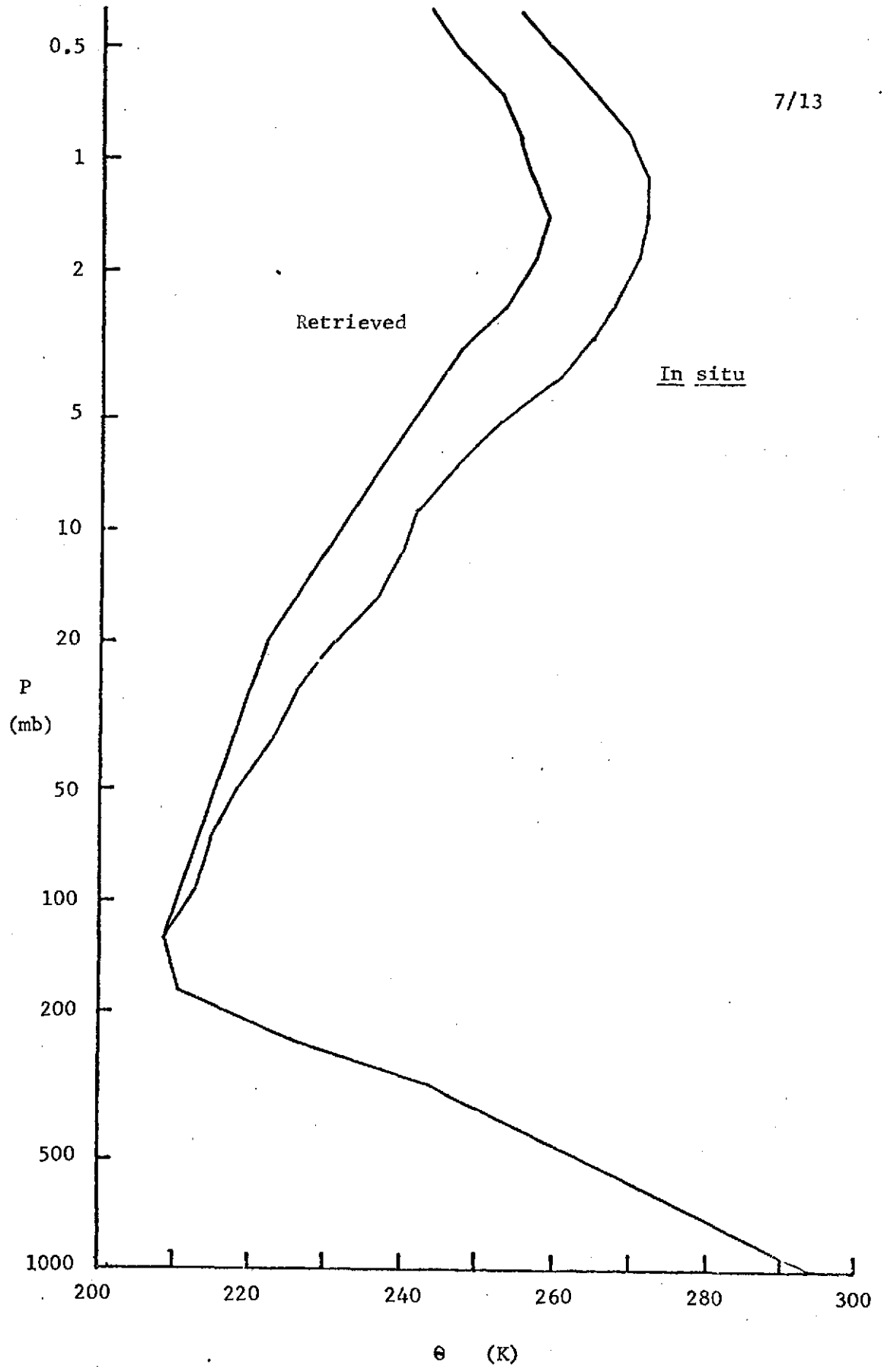
0.5
1
2
5
10
20
P
(mb)
50
100
200
500
1000
Retrieved
In situ
200
220
240
260
280
300
θ (K)

Fig. 22. The temperature profile to 100 km of the U.S. Standard Atmosphere, 1962.

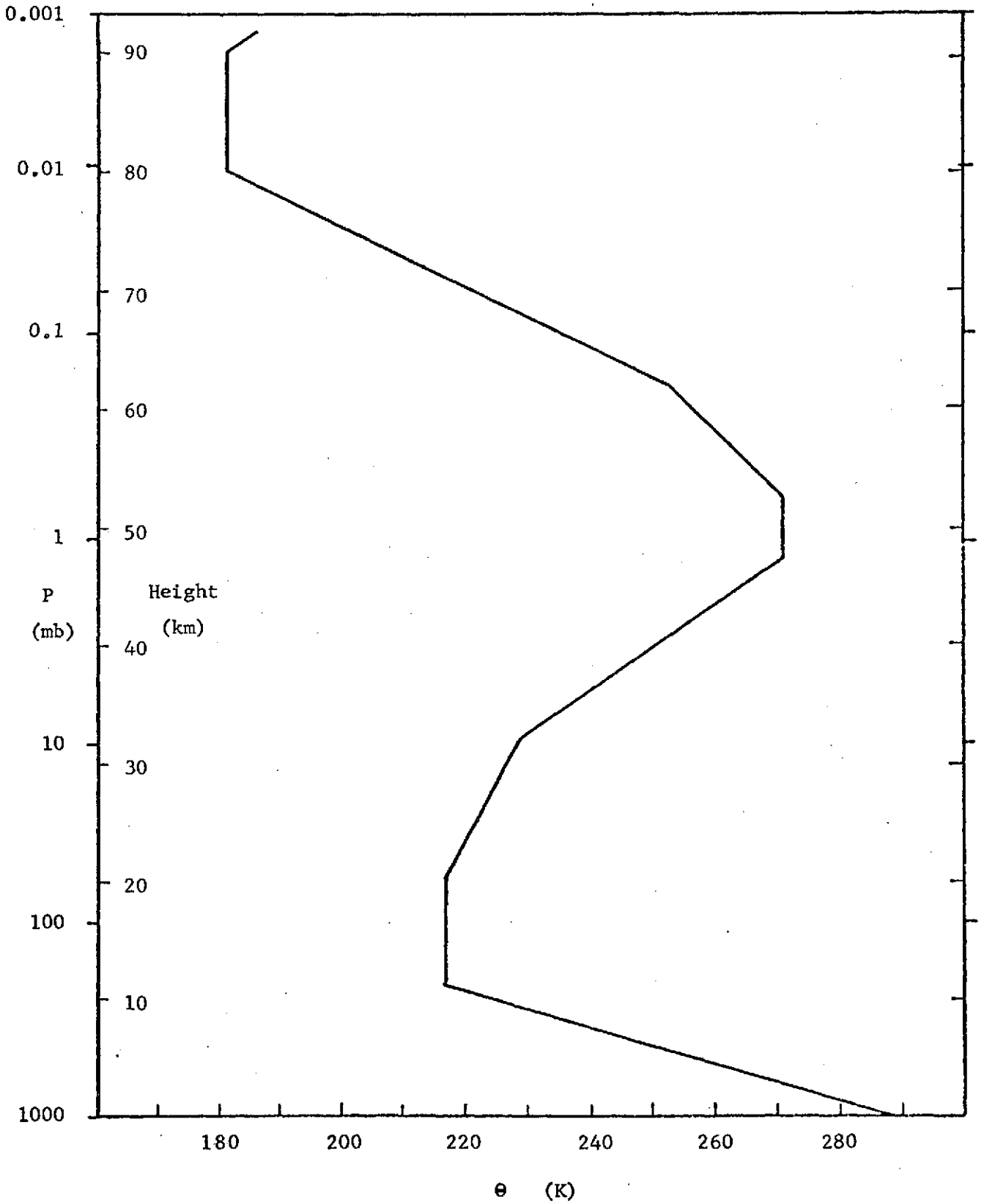
0.001
0.01
0.1
1
10
100
1000
P
(mb)
90
80
70
60
50
40
30
20
10
Height
(km)
180
200
220
240
260
280
θ (K)

APPENDIX A

CALCULATING THE OUTGOING RADIANCE

The solution of the direct problem involves evaluating (13), repeated here:

$$I(\upsilon_i) = \sum_j \sum_\ell B(\upsilon_\ell, \theta(z_j))\ \Delta\bar{T}\ (\upsilon_\ell, z_j)\ \phi(\upsilon_\ell - \upsilon_i) \qquad \text{(A-1)}$$

where z_j ($j = 1, 30$) represents the center of the j'th atmospheric layer, and υ_ℓ ($\ell = 1,800$) represents the center of the ℓ'th 0.1 cm^{-1} wide interval, which extends up to ± 40 cm^{-1} on either side of υ_i. Since (A-1) must be evaluated for each υ_i at every iteration of the relaxation procedure, a rapid but accurate algorithm is required.

The summation over ℓ (*i.e.*, the integration with respect to υ) can be done once and for all using the following approximate factoring of the blackbody function (due to Chahine, 1968). The blackbody function is:

$$B(\upsilon,\theta) = a\upsilon^3(\exp(b\upsilon/\theta) - 1)^{-1} \qquad \text{(A-2)}$$

where a and b are constants. For any υ_o and θ_o, let:

$$X(\upsilon) = a\upsilon^3 \exp(\frac{b\upsilon}{2\theta_o})$$

$$Y(\theta) = \exp(-\frac{b\upsilon_o}{2\theta})$$

$$D(\upsilon,\theta) = \exp\left[\frac{b}{2}(\frac{\upsilon}{\theta_o} + \frac{\upsilon_o}{\theta}) - \frac{b\upsilon}{\theta}\right]\left[1 - \exp(-\frac{b\upsilon}{\theta})\right]^{-1} \qquad \text{(A-3)}$$

so that

$$B(\upsilon,\theta) \equiv X(\upsilon)\ Y(\theta)\ D(\upsilon,\theta) \tag{A-4}$$

In the 15μ region ($\upsilon_o \sim 667\ cm^{-1}$) and at normal atmospheric temperatures ($\theta_o \sim 250$ K), and for υ and θ close to υ_o, θ_o, $D(\upsilon,\theta)$ is close to unity and varies quite slowly with υ and θ. In the neighborhood of υ_o, θ_o, one can write to a close approximation:

$$B(\upsilon,\theta) \simeq X(\upsilon)\ Y(\theta)\ D(\upsilon_o,\theta_o) \tag{A-5}$$

A more exact specification of the accuracy of this approximation will be given later.

Having factored the blackbody function in this way, (A-1) can be written:

$$I(\upsilon_i) = \sum_j Y(\theta(z_j))\ G(\upsilon_i,z_j) \tag{A-6}$$

where:

$$G(\upsilon_i,z_j) = D(\upsilon_i,\theta_o) \sum_\ell X(\upsilon_\ell)\ \Delta\bar{T}\ (\upsilon_\ell,z_j)\ \phi(\upsilon_\ell - \upsilon_i) \tag{A-7}$$

with υ_o set equal to υ_i and θ_o equal to any average temperature. Since the $G(\upsilon_i,z_j)$'s are independent of $\theta(z_j)$, they can be calculated once and stored. For any given temperature profile, the calculation of $I(\upsilon_i)$ requires only the summation over j, *i.e.*, integration with respect to height.

The extreme range of expected atmospheric temperatures is from about 180 K to 320 K. The factored blackbody approximation is not sufficiently accurate over this wide a temperature range. Therefore, the interval 180 K to 320 K was divided into seven smaller intervals, each 20 K wide. Within each subinterval, the factored blackbody approximation was applied and the constants (the G's) calculated. In calculating $I(\theta_i)$, each $\theta(z_j)$ is first examined to see in which subinterval it falls: the appropriate stored constants are then used in summing over z_j.

To check the accuracy of the factored blackbody approximation, it was compared to a brute force integration with respect to θ. The radiances computed by the two methods differ by 0.2 percent or less. Since the measured radiances have an uncertainty of about 1 percent, the accuracy of the factored blackbody method is sufficient for this study.

The numerical integration with respect to z is performed using a simple trapozoidal rule. The vertical step size is about 2 km with 31 grid points (including the boundary term). In order to determine whether this grid spacing provides sufficient accuracy, the following tests were performed. A transmission function of the form $\bar{T} = \exp(-cP)$ was assumed, with 1/c equal to 3 mb and 78 mb (*i.e.*, corresponding to weighting functions peaking at 3 mb and at 78 mb). The outgoing radiance was calculated by numerical integration using three different step sizes: 2 km, 1 km, and 0.1 km. A standard temperature profile was assumed at the 2 km grid points: the temperature at points in between for the other step sizes was found by linear interpolation. The effective temperature of each layer was taken as the temperature at the middle of each layer. The difference between the

radiances calculated with grid sizes of 2 km and 0.1 km was less than 0.2 percent, showing that the 2 km grid size is fine enough for this study.

The combined quadrature error for the factored blackbody approximation and for the vertical grid size of 2 km is about 0.4 percent, compared to the measurement noise of 1 percent.

APPENDIX B

DETERMINING THE EFFECTIVE RADIATION TEMPERATURE $\theta(z_T)$

In this section, limits on the possible range of $\theta(z_T)$, the effective radiation temperature of the atmosphere above 58 km, will be derived and a mean value estimated.

Above 58 km, the ratio of the doppler half width to the Lorentz half width for CO_2 is about 20, and this ratio increases with height. Therefore, above 58 km, the doppler line shape is dominant. For the Q branch lines around 668 cm^{-1}, shown in Fig. 3, a rough calculation shows that saturation of the doppler core of these lines occurs at about 0.01 mb. Thus, the function $d\bar{T}/dz$ at about 668 cm^{-1} due only to the doppler line shape has a peak at about 0.01 mb ($\sim$ 80 km). When the additional factor $dB/d\theta$ is considered, the weighting function $\frac{dB}{d\theta}\frac{d\bar{T}}{dz}$ peaks somewhat below 80 km. Thus, if the transmission calculations were extended to above 58 km, the weighting functions around 668 cm^{-1} would show a small secondary peak between 80 and 58 km. From Fig. 10, one can see that there is a definite upturn at 58 km in the weighting functions at 668.8 cm^{-1} and 667.4 cm^{-1} anticipating this secondary peak. While it is impossible to say exactly at what levels these peaks will occur without a detailed calculation, clearly they will be significantly above 58 km.

The effective radiation temperature $\theta(z_T)$ of the atmosphere above 58 km is approximately the temperature at the level of this secondary peak. With this peak occurring between 58 and 80 km, the range of $\theta(z_T)$ is approximately 200 to 240 K, as seen in Fig. 22, the U.S. Standard Atmosphere,

1962. The problem remains to determine the best value. Note that the absorption above 58 km at 648.6 cm^{-1} and 654.9 cm^{-1} is only 1.7 percent and 0.5 percent respectively, so that the choice of $\theta(z_T)$ is not critical for these weighting functions. Inversions performed with different values of $\theta(z_T)$ confirm that the retrieved temperatures for these weighting functions depend only weakly on $\theta(z_T)$.

Also, since the weighting functions at 668.1 cm^{-1} and 667.4 cm^{-1} both view about the same spectral region around the 15μ Q branch, the emission in both channels from above 58 km is due to the same lines and should come from the same region of the atmosphere. This conclusion is supported by the fact that the absorption at these two wavenumbers above 58 km, 9.0 percent and 4.9 percent respectively, is very nearly in the same ratio as the ratio of the unapodized to the apodized instrument functions (normalized). Therefore, $\theta(z_T)$ for 668.1 cm^{-1} and for 667.4 cm^{-1} should be the same. This value will do for the other weighting functions also, since the value of $\theta(z_T)$ is not critical for these channels.

I had hoped to select the best value of $\theta(z_T)$ using the following procedure: υ_4 (667.4 cm^{-1}, apodized) sounds most of the stratosphere but is not relaxed. It, therefore, serves as a check on the internal consistency of the retrieved profile: if the retrieved profile converges on the exact profile, then the residual R_4 should converge to zero. The optimum value of $\theta(z_T)$ should, therefore, be the one which minimizes the average of the R_4's. Note that this conclusion is based on several assumptions: in particular, 1) that there are no systematic errors in the data, and, 2) that the effect of the day-to-day variation in $\theta(z_T)$ is small.

However, experiments with inversions showed that R_4 is very nearly independent of $\theta(z_T)$; increasing $\theta(z_T)$ leads to decreased retrieved temperatures at most levels, which almost exactly offsets the increase in I_4 due to the change in $\theta(z_T)$. The average value of R_4 for the nine cases is 3.1 percent, with a standard deviation of 1.1 percent, showing that the bias in R_4 is systematic and not random. The possible reasons for the bias in R_4 will be dealt with later.

In an attempt to remove the bias in R_4, two simultaneous values for $\theta(z_T)$ were tried, one for I_4 alone and another, higher value for the other radiances. The supposition was that the emission from the top layer might come from a somewhat higher level for I_4 than for the other channels. Two values of $\theta(z_T)$ which lead to an average R_4 of zero were 200 K and 245 K. However, from the previous discussion, it does not appear that this large a difference in the two effective emission temperatures can be justified theoretically.

The choice of $\theta(z_T)$ must be made on the basis of intuition and the reasonableness of the profiles it produces. The effective level of emission lies between 58 km and 80 km, giving a possible range of temperature of about 200 K to 240 K. Using 70 km as a reasonable estimate for the effective emission level leads to a value for $\theta(z_T)$ of 220 ± 20 K.

Fortunately, the sensitivity of the retrieved profiles to $\theta(z_T)$ is not great. Increasing $\theta(z_T)$ from 220 to 240 K causes a systematic decrease in the retrieved temperature at z_1 of 2.0 ± 0.2 K, a decrease at z_2 of 0.2 ± 0.3 K, and an increase at z_3 of 0.3 ± 0.2 K. Decreasing $\theta(z_T)$ from 220 K to 200 K leads to similar but opposite changes in the retrieved

temperatures. The uncertainty in the retrieved temperatures due to the uncertainty in $\theta(z_T)$ is then, ±2.0 K at z_1, ±0.3 K at z_2, and ±0.3 K at z_3.